Graphical and Stage-to-Stage Methods for Reactive Distillation Column Design

Oscar Sánchez Daza
Dept. de Ingeniería de Procesos e Hidráulica, Universidad Autónoma Metropolitana-Iztapalapa, México, D.F., C.P. 09340
and
Centro de Química, Instituto de Ciencias de la Universidad Autónoma de Puebla, México

Eduardo S. Pérez-Cisneros
Dept. de Ingeniería de Procesos e Hidráulica, Universidad Autónoma Metropolitana-Iztapalapa, México, D.F., C.P. 09340

Erik Bek-Pedersen and Rafiqul Gani
CAPEC, Dept. of Chemical Engineering,
Technical University of Denmark, 2800, Lyngby, Denmark

Based on the element mass-balance concept, three graphical methods and one stage-to-stage computation method for design of reactive distillation columns have been developed. The element-based approach allows the design of reactive distillation columns by using simple tools similar to those that are typically employed for nonreactive systems. For example, simple design methods employing reactive McCabe-Thiele- and reactive Ponchon-Savarit-type diagrams for design of reactive distillation of binary-element systems — which may be ternary or higher in terms of mixture compounds — are presented. Also, the driving-force approach has been extended to employ the element concept for reactive systems. For multielement systems, the design is performed by employing a stage-to-stage computation method. For combined reactive distillation columns, comprising both reactive and nonreactive stages, a simple design strategy is proposed, based on the stage-to-stage computation method considering reactive and nonreactive bubble-point calculations. This strategy tracks the conversion or generation and temperature between the feed and the end stages of the column, and indicates when and where nonreactive stages should be added to a reactive distillation column in order to achieve the desired separation. Illustrative examples highlight the application of the design methods, as well as the verification of such designs through rigorous simulation.

Introduction

In recent years, reactive distillation has become a highly promising hybrid process for many combined reaction–separations schemes. The application of this combined reaction–separation process has been considered to be useful only for reactive systems limited by chemical equilibrium, and it has been applied successfully to methyl acetate and methyl-*tert*-butyl ether (MTBE) production (Agreda et al., 1990; Smith and Huddleston, 1982). However, it has recently been claimed (Pérez-Cisneros et al., 2002) that reactive distillation also may be applicable to processes involving complex nonequilibrium limited reactive systems, such as diesel and gasoline hydrodesulfurization.

The increasing interest in reactive distillation has been accompanied by the development of various simulation algorithms related to the study of operation and control of the process (Abufares and Douglas, 1995; Monroy et al., 2000). The design of reactive distillation columns (RDC) has also received some attention. Most of the existing work related to design of RDC is based on the use of the transformed com-

Correspondence concerning this article should be addressed to R. Gani.

position variables proposed by Doherty (Barbosa and Doherty, 1988; Doherty and Buzad, 1992; Espinosa et al., 1993, 1995, 1996; Ung and Doherty, 1995; Bessling et al., 1997). Barbosa and Doherty (1988) developed a technique for designing single-feed and double-feed RDC with the assumption of constant molar overflow. Espinosa et al. (1993) proposed using Ponchon-Savarit diagrams in the transformed composition enthalpy space to simultaneously account for heat and mass balance, assuming reaction equilibrium. Doherty and Buzad (1992) continued their studies with kinetically controlled reactions in terms of the Damköhler number. Recently, Chaddha et al. (2001) have performed an interesting study of the effect of chemical kinetics on feasible splits in reactive distillation. Another approach for designing RDC was proposed by Gumus and Ciric (1997), where the design problem is formulated as a mixed-integer nonlinear bilevel optimization problem. Recently, Lee et al. (2000) proposed graphical methods to illustrate how to distribute reaction zones in an RDC based on the *difference-points* concept. Such points are referred to as the points of intersection of the reactive operating lines and the 45-degree line of a *y-x* diagram. Despite the extension of the difference-points concept to consider the heat effect and multicomponent reactive systems in a RDC (Lee et al., 2001a,b; Lee and Westerberg, 2001; Hoffmaster and Hauan, 2001), such methods, while easy to apply for two-compound reactive systems (that is, isomerization reactions), become more difficult for higher dimension problems.

The objective of the present work is to introduce a set of design methods for RDC that are simple, easy to use, and similar in concept to nonreactive distillation design methods. The methods are based on the element concept (Pérez-Cisneros et al., 1997), which significantly reduces the dimension and complexity of the intrinsic calculation problem, aids in defining the design goals, and in solving the design problem. The methods developed are similar to those typically employed for nonreactive systems (Seader and Henley, 1998). For binary element systems, which can be ternary or higher in terms of mixture compounds, a simple reactive *McCabe-Thiele*-type method, assuming constant total element mass overflow (CTEMO), which does not mean constant component-based molar overflow and a reactive *Ponchon-Savarit*-type of method accounting for heat effects, has been developed. For an energy-efficient design, the driving-force approach of Gani and Bek-Pedersen (2000) has been extended to include reactive systems. For the design of ternary element systems, which are usually quaternary or higher in terms of mixture compounds, a reactive stage-to-stage calculation method is presented. For *combined* RDC, comprising reactive and nonreactive stages, the stage-to-stage procedure is used. The methods have been tested in a systematic manner with many reactive systems. In this article, results from four case studies highlighting the application of the design methods and, in some cases, the verification of the design through rigorous simulations are presented.

Element Balances and Equilibrium Condition

In the design of an RDC under equilibrium conditions, the computation of the chemical–physical equilibrium (CPE) is an important step. Using the element concept (Pérez-Cisneros et al., 1997), a multicomponent CPE problem is transformed into a phase equilibrium problem for a mixture of elements (representing the system). In the element-based approach, the CPE problem is solved by minimizing the Gibbs energy of the reactive system

$$\min G(\boldsymbol{n}) = \sum_{\beta=1}^{NP} \sum_{i=1}^{NC} n_i^{\beta} \mu_i^{\beta} \tag{1}$$

Subject to the M constraints

$$\sum_{\beta=1}^{NP} \sum_{i=1}^{NC} A_{j,i} n_i^{\beta} - b_j = \mathbf{0} \qquad j = 1, 2, \ldots, M \tag{2}$$

where $G(\boldsymbol{n})$ is the total Gibbs energy of a system containing NC species and NP phases. Equation 2 represents the M independent element mass balances, with the coefficient A_{ji} being the number of times the reaction invariant element j is present in molecule i. The solution of this constrained optimization problem can be obtained through the Lagrange multiplier formulation, where the relation between the Gibbs free energy and the Lagrange multipliers is exploited for a robust method of solution (Pérez-Cisneros, 1997). Thus, a fully consistent thermodynamic description of a chemically equilibrated phase is obtained in terms of $\boldsymbol{b}$, the (element) composition vector, and $\boldsymbol{\lambda}$, the corresponding element potential vector. The procedure for identifying the elements is based on the determination of the minimum number of elements and for each element, the fragment (a combination of atoms present in the compounds, for example, "CH2," that may be part of a molecule or a whole molecule) that can represent it so that the atomic balance for all compounds (including inert compounds) in the reactive system can be satisfied. The minimum number of elements is usually the number of compounds (reactants and products) involved in the reactions minus the number of reactions plus the number of inert compounds. A more detailed description of this procedure is given by Pérez-Cisneros (1997).

Design of Reactive Distillation Columns

The design methods are divided in terms of the number of elements involved. Three graphical design methods for binary element (reactive) systems have been developed and a stage-to-stage calculation method is used for ternary (or higher) element (reactive) systems.

Binary element reactive systems

Consider a full RDC, that is, all stages are reactive stages except the condenser, operating under CPE conditions (see Figure 1). The feed is a mixture of two elements A and B ($j = A, B$). In the case of a binary element reactive distillation, the reactive stripping section concentrates the less-volatile element (B) in a liquid stream, while the reactive rectifying section concentrates the more-volatile element (A) in the vapor stream. Usually, the most volatile compounds are associated with the most-volatile element (A). This is true when the elements actually represent a whole molecule. However, when the elements only partially represent a

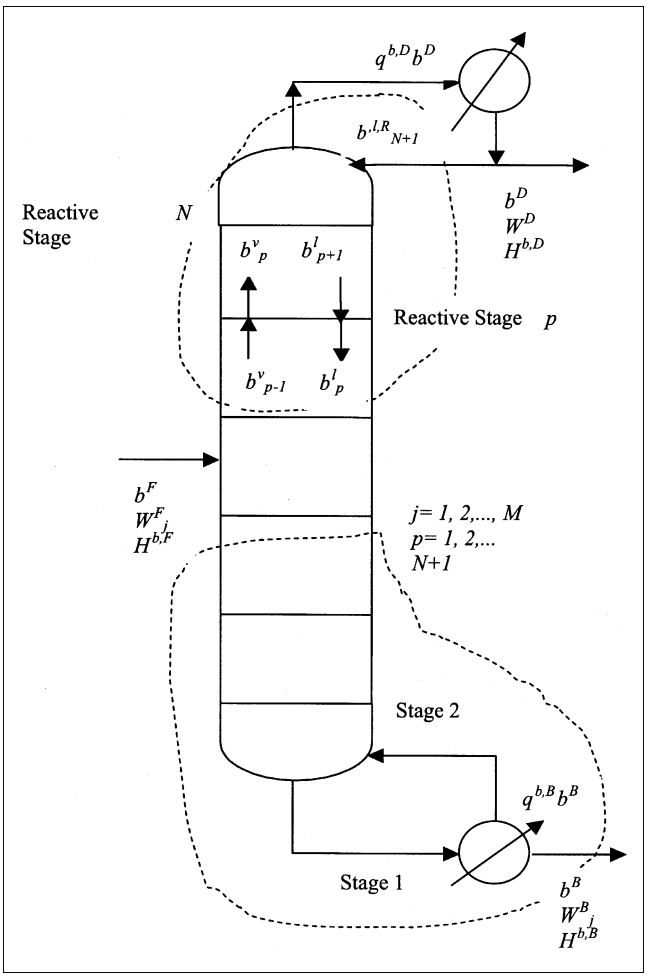

Figure 1. Full reactive distillation column (RDC).

molecule, then the volatility of the element is assigned by the volatility of the molecule it is representing (see, for example, the reacting system in benzene production).

Based on the fact that the elements, or atoms, must be conserved, both when chemical reactions occur or not, the element mass balances for the column in Figure 1 can be written as (see the "Notation" section for a definition of the variables)

Around the column

$$b^F = b^B + b^D \tag{3}$$

$$b^F W_j^F = b^B W_j^B + b^D W_j^D \qquad j = 1, 2, \ldots, M \tag{4}$$

$$\text{Element reflux} = RR = \frac{b^{l,R}_{N+1}}{b^D} \tag{5}$$

Stripping section

$$b^{l,S}_{p+1} = b^{v,S}_p + b^B \tag{6}$$

$$b^{l,S}_{p+1} W^l_{j,p+1} = b^{v,S}_p W^v_{j,p} + b^B W^B_j \tag{7}$$

Rectifying section

$$b^{v,R}_p = b^{l,R}_{p+1} + b^D \tag{8}$$

$$b^{v,R}_p W^v_{j,p} = b^{l,R}_{p+1} W^l_{j,p+1} + b^D W^D_j \tag{9}$$

where

$$W^l_j = \frac{\sum_{i=1}^{NC} A_{j,i} x_i}{\sum_{i=1}^{NC} \sum_{j=1}^{M} A_{j,i} x_i} \tag{10}$$

$$W^v_j = \frac{\sum_{i=1}^{NC} A_{j,i} y_i}{\sum_{i=1}^{NC} \sum_{j=1}^{M} A_{j,i} y_i} \tag{11}$$

and the relations between the total element flows (b^l,b^v) and the total component-based molar flows (L,V) are given by

$$b^1 = L \sum_{i=1}^{NC} \sum_{j=1}^{M} A_{j,i} x_i \tag{12}$$

$$b^v = V \sum_{i=1}^{NC} \sum_{j=1}^{M} A_{j,i} y_i \tag{13}$$

The element energy balances for the different sections can be written as

Around the column

$$H^{b,F} b^F + q^{b,B} b^B = H^{b,B} b^B + H^{b,D} b^D + q^{b,D} b^D \tag{14}$$

Stripping section

$$H^{b,l}_{p+1} b^{l,S}_{p+1} = H^{b,v}_p b^{v,S}_p + \left(H^{b,B} - q^{b,B}\right) b^B \tag{15}$$

Rectifying section

$$H^{b,v}_p b^{v,R}_p = H^{b,l}_{p+1} b^{l,R}_{p+1} + \left(H^{b,D} + q^{b,D}\right) b^D \tag{16}$$

and the relations between the element-based enthalpy ($H^{b,l}$, $H^{b,v}$) and the component-based molar enthalpy (H^l, H^v) are given by

$$H^{b,l} = \frac{H^l}{\sum_{i=1}^{NC} \sum_{j=1}^{M} A_{j,i} x_i} \tag{17}$$

$$H^{b,v} = \frac{H^v}{\sum_{i=1}^{NC} \sum_{j=1}^{M} A_{j,i} y_i} \tag{18}$$

It should be noted that the heat of reaction is implicitly accounted for through the reference state considered for the component-based enthalpy evaluation, in this case, the elemental state. Therefore, the heat-of-reaction term is not used in the energy balance equations just given.

Step 1. Give W_j^l and P

Step 2. Guess T

Step 3. Solve for component moles n_i^l in the liquid phase (chemical equilibrium)

$$W_j^l \sum_{k=1}^{M} \sum_{i=1}^{NC} A_{ki} n_i^l - \sum_{i=1}^{NC} A_{ji} n_i^l = 0 \qquad \text{for } j = 1, 2, \ldots, M$$

$$\sum_{i=1}^{NC} \upsilon_{i,k}\, \mu_i^l = 0 \qquad \text{for } k = 1, 2, \ldots, NR$$

Step 4. Compute vapor mole fractions y_i at equilibrium

$$f_i^v - f_i^l = 0 \qquad \text{for i} = 1, 2, \ldots, NC$$

Step 5. Calculate a correction for temperature using the check equation

$$\sum_{i=1}^{NC} y_i - 1 = 0$$

if nonconverged, return to step 3.

Step 6. Compute element mole fractions for the vapor phase

$$W_j^v = \frac{\sum_{i=1}^{NC} A_{ji} y_i}{\sum_{k=1}^{M} \sum_{i=1}^{NC} A_{ki} y_i}$$

Figure 2. Algorithm 1: Reactive bubble-point algorithm.

The reactive equilibrium curve and the driving force diagram

A reactive equilibrium curve is the locus of points in both chemical and physical equilibrium. For a given element liquid composition, W_A^l, it gives the corresponding equilibrium vapor composition, W_A^v, and vice versa. A reactive equilibrium stage, p, is represented as a point on the reactive equilibrium curve where $W_{A,p}^l$ and $W_{A,p}^v$ are the liquid and vapor element compositions leaving the stage. The reactive equilibrium curve is constructed through sequential computation of reactive bubble points (see Figure 2). Typical reactive equilibrium curves are shown in Figures 3 and 4.

A driving-force diagram (see Figure 5) can be used to visualize how the operation of an RDC should be carried out in order to achieve the desired separation with the least energy consumption. On the basis of these diagrams, estimates for the important design variables, such as the number of reactive stages, element reflux ratio, and feed-stage location, are obtained (see the "Reactive Driving-Force Approach" section).

Constant total element mass-overflow assumption

For some reactive systems, it is (at least) approximately correct to apply the assumption of constant total element mass overflow (CTEMO). The change in vapor rate from stage to stage can then be derived by writing the energy balance for any reactive stage as

$$b_p^v - b_{p+1}^v = \frac{b_{p+1}^v \left(H_{p+1}^{b,v} - H_p^{b,v}\right) - b_p^l \left(H_p^{b,l} - H_{p-1}^{b,l}\right)}{\left(H_p^{b,v} - H_{p-1}^{b,l}\right)} \qquad (19)$$

It follows that there are two possible conditions that will cause the total element mass vapor flow, b^v, to be constant from stage to stage

Condition 1

$$H^{b,v} = \text{constant} \qquad H^{b,l} = \text{constant} \qquad (20)$$

Condition 2

$$\frac{\left(H_{p+1}^{b,v} - H_p^{b,v}\right)}{\left(H_p^{b,l} - H_{p-1}^{b,l}\right)} = \frac{b_p^l}{b_{p+1}^v} = \text{constant} \qquad (21)$$

From condition 2, if b^v is constant, it follows that b^l is constant. It should be noted that the enthalpies for the dif-

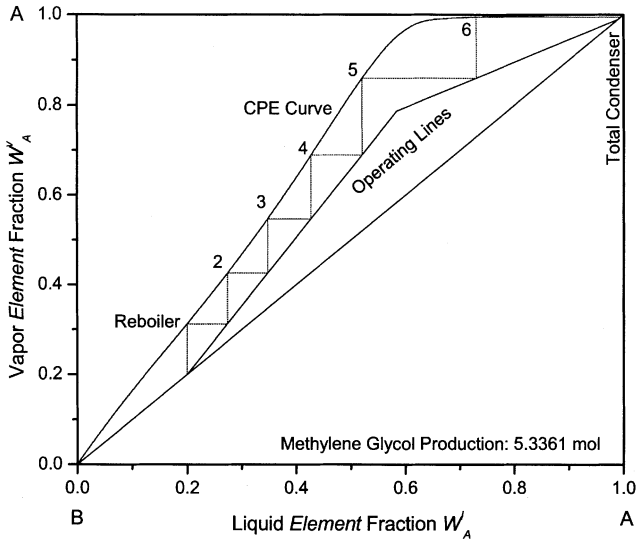

Figure 3. Reactive element McCabe-Thiele diagram: reactive system 1.

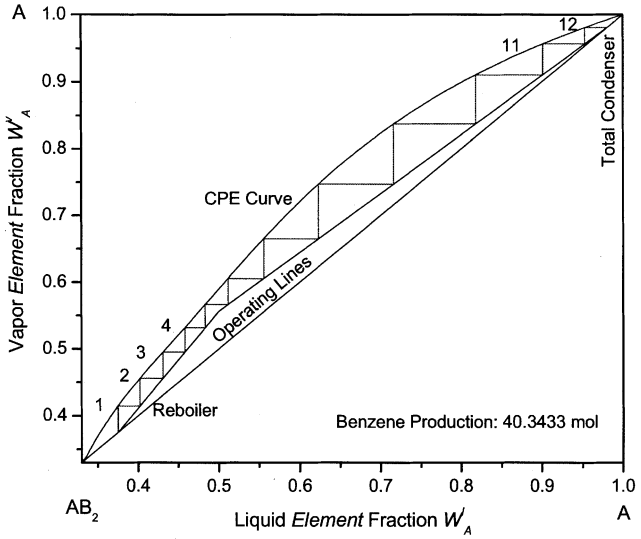

Figure 4. Reactive element McCabe-Thiele diagram: reactive system 2.

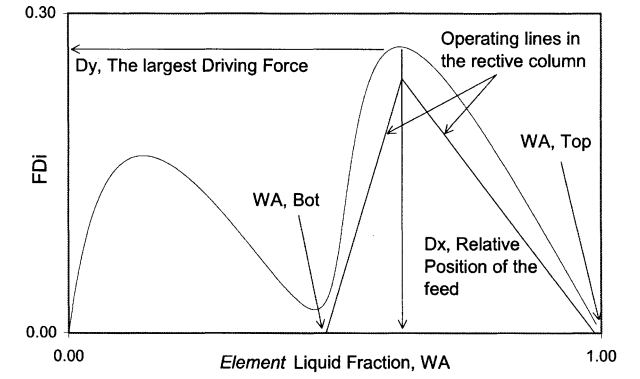

(a)

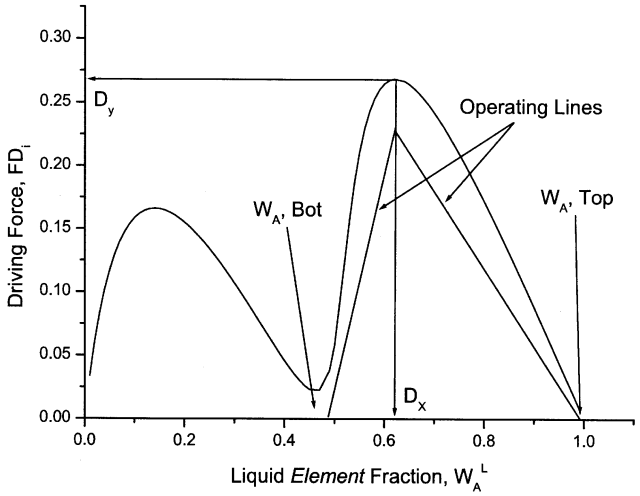

(b)

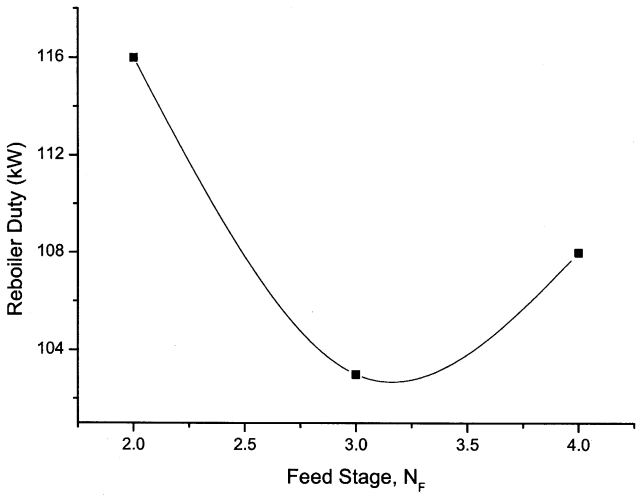

(c)

Figure 5. (a) Reactive driving-force diagram: reactive system 3a; (b) reactive driving-force diagram: reactive system 3a; (c) reboiler duty vs. feed stage: reactive system 3a.

ferent phases are element-based. From condition 1, it can be seen that CTEMO assumption will occur if the element mass heats of vaporization of elements A and B are identical, if sensible-heat contributions due to temperature changes from stage to stage are negligible, if there are no enthalpy-of-mixing effects, or if the heat of reaction is negligible. However, it should be observed that the assumption of CTEMO does not mean constant component-based molar overflow, as indicated by Eqs. 12 and 13.

The reactive McCabe-Thiele diagram

Consider the rectifying section of a full RDC (see Figure 1), by performing an element mass balance around this section for element A, Eq. 9 can be written as

$$W^{l}_{A,p+1} = \frac{b^{v,R}}{b^{l,R}} W^{v}_{A,p} - \frac{b^{d}}{b^{l,R}} W^{d}_{A} \tag{22}$$

Equation 22 represents the reactive operating line for the rectifying section. At the point where the feed is introduced to the column (intersection between operating lines), the element flows in the rectifying and stripping sections must change because of the feed entry. The element flows below the feed point (stripping section) are labeled $b^{l,S}$ and $b^{v,S}$. Performing an element mass balance for element A around the stripping section (Eq. 7) leads to the reactive operating line for the stripping section

$$W^{l}_{A,p+1} = \frac{b^{v,S}}{b^{l,S}} W^{v}_{A,p} + \frac{b^{B}}{b^{l,S}} W^{B}_{A} \tag{23}$$

Equations 22 and 23 can be simultaneously solved in order to find the intersection point of the operating lines

$$W^{l,I}_{A} = \frac{b^{D} V^{D}_{A} / b^{v,R} + b^{B} W^{B}_{A} / b^{v,S}}{b^{l,S}/b^{v,S} - b^{l,R}/b^{v,R}} \tag{24}$$

$$W^{v,I}_{A} = b^{l,R} W^{l,I}_{A} / b^{v,R} + b^{D} W^{D}_{A} / b^{v,R} \tag{25}$$

Given the necessary feed and product specifications, Eqs. 22–25 can be used to design an RDC considering two elements under CPE conditions. The detailed design procedure is given in Figure 6.

Accounting heat effects: The reactive Ponchon-Savarit diagram

An element-based enthalpy-composition diagram can also be constructed through the sequential calculation of reactive bubble points and evaluating the corresponding element enthalpies with the resulting component compositions. The following element-based enthalpy-composition curves can be obtained

$$H^{b,v}_{CPE} = f\left(W^{v}_{A,CPE}\right) \tag{26}$$

$$H^{b,l}_{CPE} = f\left(W^{l}_{A,CPE}\right) \tag{27}$$

By combining Eqs. 3–9 and 14–16, the element-based reactive operating lines and the other necessary relations for the

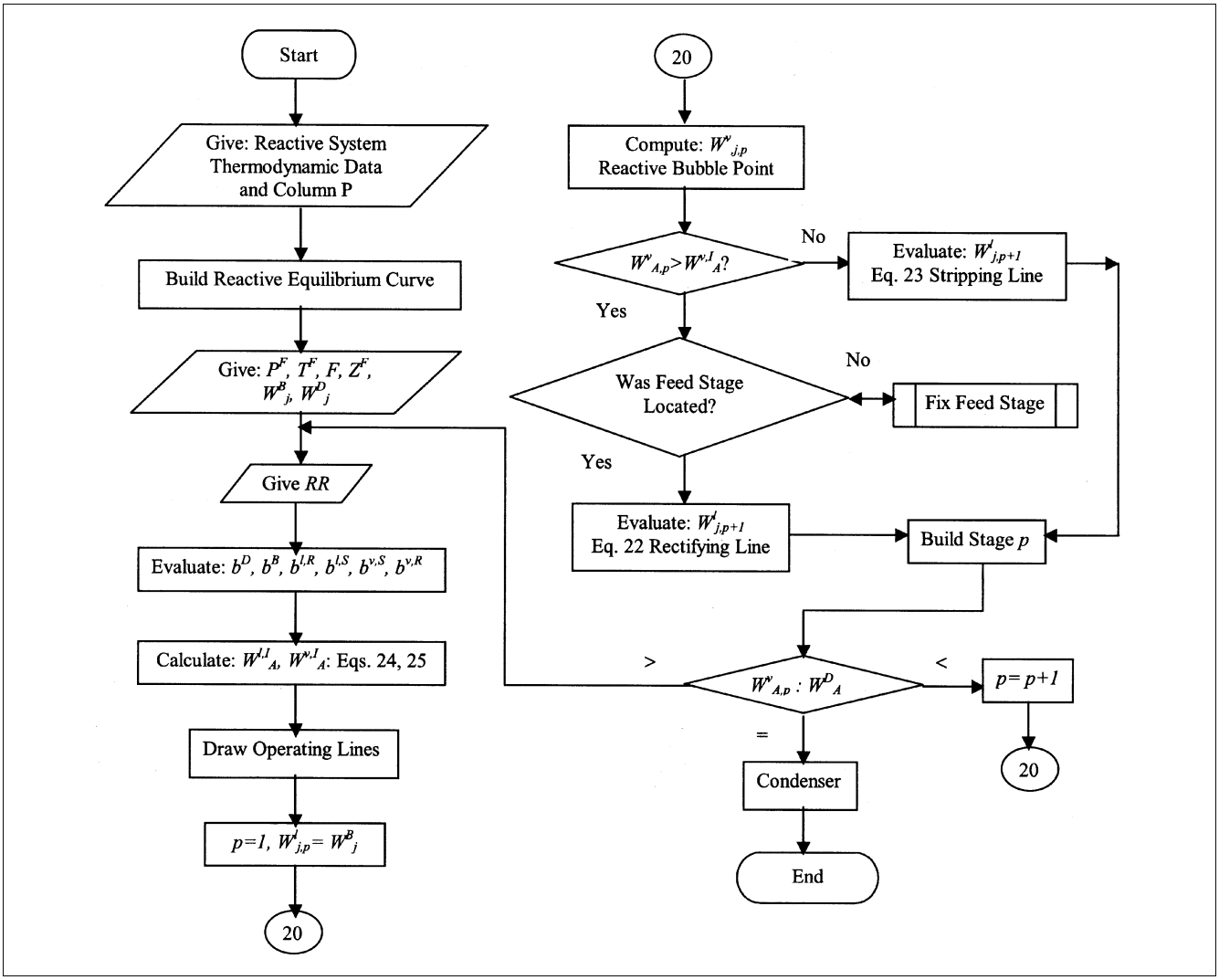

Figure 6. Algorithm 2: reactive McCabe-Thiele method.

Ponchon-Savarit diagram can be obtained, thus

Rectifying Section

$$H^{b,l}_{p+1} = \Delta D + \left(\Delta D - H^{b,v}_p\right)\frac{W^l_{A,p+1} - W^D_A}{W^D_A - W^v_p} \tag{28}$$

$$b^{v,R}_p = \frac{W^D_A - W^l_{A,p+1}}{W^v_{A,p} - W^l_{A,p+1}} b^D \tag{29}$$

Stripping Section

$$H^{b,l}_{p+1} = \Delta B + \left(\Delta B - H^{b,v}_p\right)\frac{W^l_{A,p+1} - W^B_A}{W^B_A - W^v_{A,p}} \tag{30}$$

$$b^{v,S}_p = \frac{W^l_{A,p+1} - W^B_A}{W^v_{A,p} - W^l_{A,p+1}} b^B \tag{31}$$

Overall Energy Balance

$$H^{b,OB} = \Delta D + (\Delta B - \Delta D)\frac{W^D_A - W_A}{W^D_A - W^B_A} \tag{32}$$

Condenser

$$\Delta D = H^{b,v}_N + \left(H^{b,v}_N - H^{b,D}\right)RR \tag{33}$$

Reboiler

$$\Delta B = H^{b,F} - \frac{b^D}{b^B}(\Delta D - H^{b,F}) \tag{34}$$

where

$$\Delta D = H^{b,D} + q^{b,D} \quad \text{and} \quad \Delta B = H^{b,B} - q^{b,B} \tag{35}$$

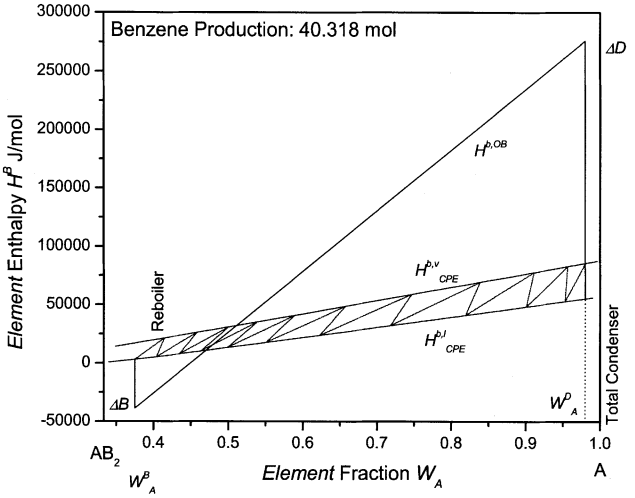

Figure 7. Reactive element Ponchon-Savarit diagram: reactive system 2.

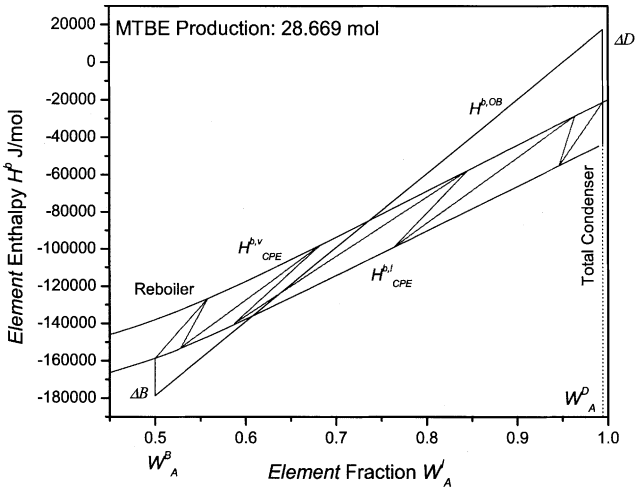

Figure 8. Reactive element Ponchon-Savarit diagram: reactive system 3a.

Based on Eqs. 26–35, the reactive Ponchon-Savarit diagram can be used to design an RDC, for two elements and the heat effects under CPE conditions. Figures 7 and 8 show two examples of reactive Ponchon-Savarit diagrams constructed by using Figure 9.

The reactive driving-force approach

The driving force approach (Gani and Bek-Pedersen, 2000) provides a design method for simple nonreactive distillation columns. In this article we have extended this methodology to include reactive systems. The driving force is defined as the difference in composition between two coexisting phases, and can be modeled by the following equation

$$F_{Di} = y_i - x_i = \frac{x_i \alpha_{ij}}{1 + x_i(\alpha_{ij} - 1)} - x_i \tag{36}$$

or in terms of elements

$$F^b_{Di} = W^v_i - W^l_i = \frac{W^1_i \alpha^b_{ij}}{1 + W^l_i(\alpha^b_{ij} - 1)} - W^l_i \tag{37}$$

The concept of operating at the largest driving force, based on Eq 37. forms the basis of the extended-design method for element reactive distillation columns, in a similar way as for nonreactive systems. It should be pointed out that the calculations are all based on chemical elements. The location of the largest driving force can be obtained from the derivative of the driving force model (Eq. 37) with respect to the liquid element composition. The expression is given by

$$\frac{dF^b_{Di}}{dW^l_i} = \frac{\alpha^b_{ij}}{\left(1 - W^l_i - W^l_i \alpha^b_{ij}\right)^2} - 1 \tag{38}$$

The driving-force design method for reactive as well as nonreactive distillation systems is based on the availability of data for the vapor–liquid behavior (equilibrium or not). In the case of reactive systems, as treated in this article, the vapor–liquid equilibrium data must be based on the element. This is because the driving-force diagram can only exploit binary interaction between compounds (or elements) in two coexisting phases, or two compounds on a solvent-free basis. Note that the element-based driving-force diagram fully incorporates the extent of reaction on an element basis, and, therefore, it can be applied in the design of RDC.

Provided the element vapor–liquid behavior data exist, or can be computed, the reactive driving-force diagram can be computed. This design method will, as pointed out by Gani and Bek-Pedersen (2000) for nonreactive systems, lead to a near-optimum configuration with respect to energy consumption. From this simple reactive driving-force diagram, essential design parameters, such as feed-stage location and minimum reflux ratio, can be obtained in a simple graphical way. The description of the driving-force-based reactive-distillation design method is given in detail in Figure 10.

Ternary element reactive systems

Similar to the multicomponent nonreactive mixtures, the graphical design methods may not be applied in a straightforward way. Therefore, the design of reactive distillation columns for ternary-element reactive systems should be performed through a stage-to-stage calculation method. However, in this case, it is necessary to specify a set of design variables that satisfy the degrees of freedom, and the choice of this set of variables can be carried out through the analysis of the reactive residue curve maps.

In this work, the stage-to-stage computation method developed is based on the *Lewis-Matheson* method (Lewis and Matheson, 1932), which has been adapted for reactive systems. Therefore, for any reactive ternary-element system, given the column pressure, feed and product specifications, and reflux ratio, the reactive Lewis-Matheson method consists of two basic steps:

(1) Calculate, recursively, from the bottom to the top, the element compositions of the vapor and liquid phases (W^v_j, W^l_j) by performing a reactive bubble-point computation and,

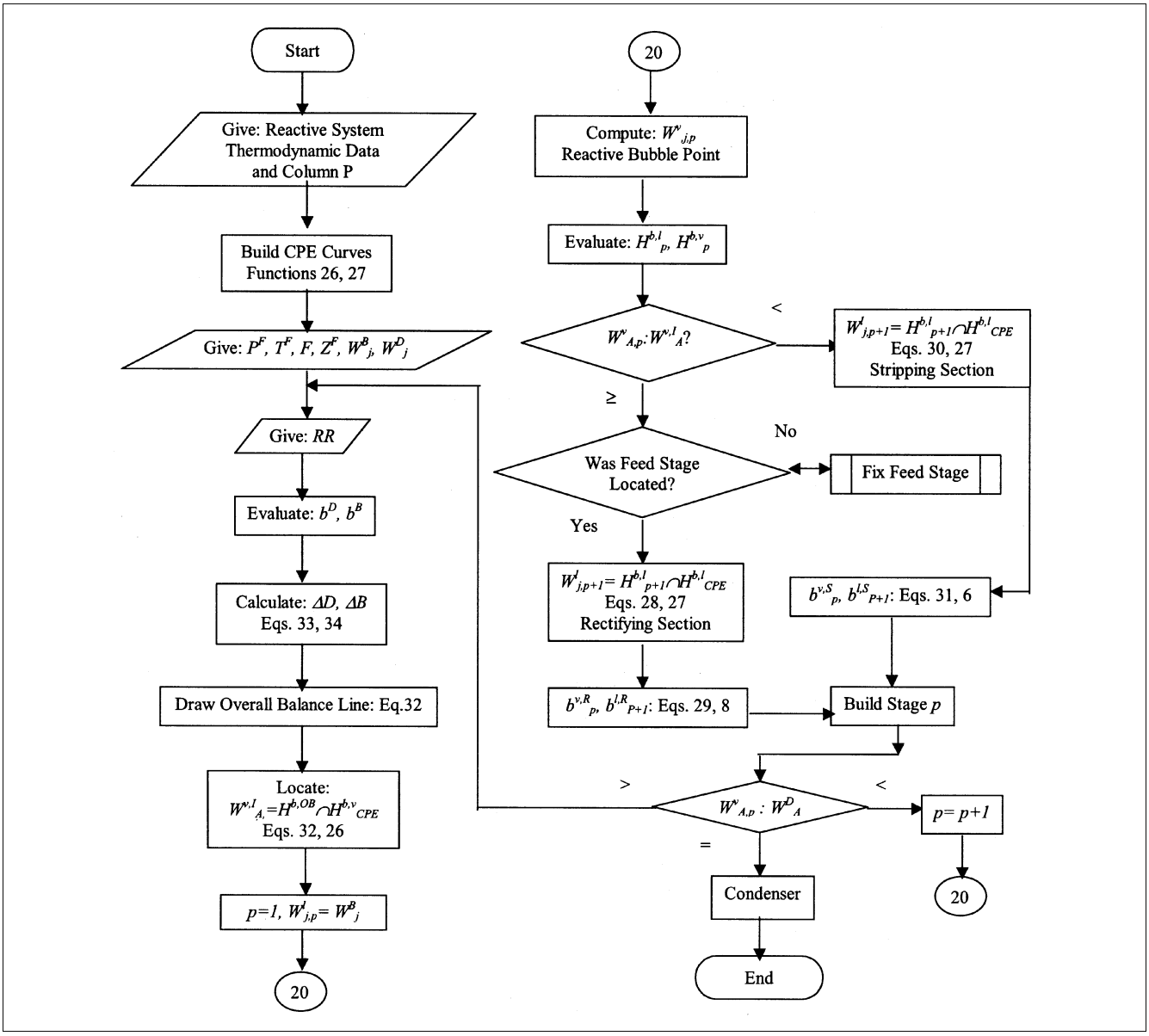

Figure 9. Algorithm 3: Reactive Ponchon-Savarit method.

(2) With this information, calculate the element flows by means of the following equations

$$b^v_{p+1} = b^v_p + b^{F,v}_{p+1} \tag{39}$$

$$b^l_{p+1} = b^v_p + b^l_p - b^v_{p-1} - b^{F,l}_p - b^{F,v}_p \tag{40}$$

$$W^l_{j,p+1} = \left(b^v_p W^v_{j,p} + b^l_p W^l_{j,p} - b^v_{p-1} W^v_{j,p-1} - b^{F,l}_p W^{F,l}_{j,p} - b^{F,v}_p W^{F,v}_{j,p}\right)/b^l_{p+1} \tag{41}$$

It should be pointed out that this procedure is not restricted to handling only one feed or three elements, but multiple feed and multielement reactive systems also can be manipulated. The detailed design procedure is shown in Figure 11.

Design Strategy for Combined Reactive Distillation Columns

Commonly, the operation of any reactive distillation column will consider at least one or two nonreactive sections (or stages). Since the nonreactive sections can be helpful in buffering the temperature and concentration of the streams leaving the reactive sections, the design of a combined reactive distillation column, that is, a reactive distillation column comprising reactive and nonreactive stages or sections, cannot be performed with the graphical methods developed before, including binary-element systems. This is because, while a reactive stage is considered under chemical and physical equilibrium, in the nonreactive stages only physical equilibrium occurs. Therefore, the reactive equilibrium curves used in the reactive McCabe-Thiele, Ponchon-Savarit, and driving-force diagrams cannot be used in drawing the non-

1. Check if the reactive separation can be exploited on the basis of two *elements* (possibly with inert compound(s). If yes, go to 2, otherwise stop.
2. Generate or retrieve vapor-liquid *element* data at the desired operating pressure.
3. Calculate the corresponding driving-force diagram, i.e., plot $|W_{Ai}^V - W_{Ai}^L|$ vs. W_{Ai}^L.
4. Identify the area of operation on the driving-force diagram.
4.1. Rescale the x-axis accordingly, such that the area of operation covers the [0;1] composition space.
5. Determine or specify the condition of the feed (vaporization degree).
6. Identify the points D_y and D_x (as shown in Figure 5).
6.1. Determine N_F from $N_F = (1 - D_x)N_P$.
6.2. Give the product specifications and locate the points A and B. Determine the slopes of the lines AD_y and BD_y. Determine the corresponding RR_{min}.
7. Identify whether nonreactive stages are needed (or used) below and/or on top of the reactive section in the column, i.e., identify whether A and B correspond to the final desired products on a compound basis.
7.1. If no nonreactive stages are needed, the design is now complete.
7.2. If A and/or B does not correspond to the desired compound product, nonreactive stages can be added in the top and/or bottom. The stages should be designed as individual rectifying and/or stripping sections based on the algorithm presented by Gani and Bek-Pedersen (2000).

Figure 10. Algorithm 4: Driving-force algorithm for RDC.

reactive stages, and a stage-to-stage computation procedure considering reactive and nonreactive bubble-point calculations is needed.

The strategy for the design of a combined RDC basically consists of the following three steps (given the feed and product specifications):

(1) To design a full RDC using the appropriate method (graphical or stage-to-stage) to obtain the basic design information: total number of stages required, feed-stage location, optimal reflux ratio, bottom or top product component composition, temperature, and generation profiles.

(2) To perform an analysis, from the bottom to the feed-stage point, of the temperature and generation profiles obtained in step 1. At any reactive stage, if the generation of the key component is negligible or negative, then the reaction is reversed and decomposition of such a key component (product or reactant) could occur. In that case, nonreactive stages should be introduced, and a redesign of a combined RDC using a stage-to-stage procedure with reactive and nonreactive bubble-point calculations is performed. If the new-generation profile is positive for the whole reactive section, then the number of reactive and nonreactive stages is fixed, and go to step 3.

(3) With the previously obtained combined RDC design, the analysis of the generation profile from the feed point to the top of the column is carried out. As in step 2, if the generation of the key component is negative or negligible, nonreactive stages are introduced. When the generation is positive for the whole reactive section, the nonreactive and reactive stages for the complete combined reactive distillation column are fixed.

It should be pointed out that the design strategy proposed here is based on tracking the key-component generation, and must attain values such that the reactive distillation column design is feasible. However, other variables, such as occurrence of reactive or nonreactive azeotropes and composition of any component, also could be selected to switch/add nonreactive stages. The strategy described is presented in Figure 12.

Application Examples

For the application of the design methods developed before, four reactive systems are considered: (1) methylene glycol production—highlights the application of the reactive McCabe-Thiele method; (2) Benzene production—highlights the applications of the reactive McCabe-Thiele, Ponchon-Savarit, and driving-force methods, as well as verification through rigorous simulation; (3) MTBE production with and without inert component—highlights the applications of the reactive McCabe-Thiele, Ponchon-Savarit, and Lewis-Matheson methods, as well as verification through rigorous simulation; and (4) ethanol synthesis—highlights the application of the reactive driving-force method. The reaction schemes and the element representation of the reactive systems are given in Tables 1–5 and Table 6 gives summary of resulting RDC designs for all the four examples.

For the calculations related to the reactive McCabe-Thiele, Ponchon-Savarit, Lewis-Matheson and the driving-force methods, the CPE program package (Sańchez-Daza and Pérez-Cisneros, 2002) and the ICAS program package (Gani et al., 2002) have been used. Aspen-Plus has been used for verification with rigorous simulation.

Methylene glycol production

The reaction between formaldehyde and water to produce methylene glycol and the further polymerization of methylene glycol to polyoxymethylene have been reported by Brandani and DiGiacomo (1984), Ung and Doherty (1995), and by Albert et al. (1996). The physical properties (vapor pressure) data, the UNIFAC model parameters for the computation of the liquid-phase activity coefficients and the temperature-dependent equilibrium constant are taken from Albert et al. (1996). Since the Gibbs free energies of formation for methylene glycol and poly-oxymethylene could not be found in the open literature, it was decided to use the chemical equilibrium constants given by Albert et al. (1996) to estimate the missing values. The element representation of the reactive system is given in Table 1.

Figure 3 shows the reactive equilibrium curve and the reactive operating lines employed for a quick configuration of a full reactive-distillation column for the production of methylene glycol based on a reactive McCabe-Thiele diagram. The feed and product specifications, and the operation pressure are given in Table 7. The main objective in the design of this reactive-distillation column is to obtain a mixture of methylene glycol and water as a bottom product. Note that the undesired polymerization side reaction inhibits high yield. From Figure 3 it can be observed that at values of $W_A^l \geq 0.7$ any

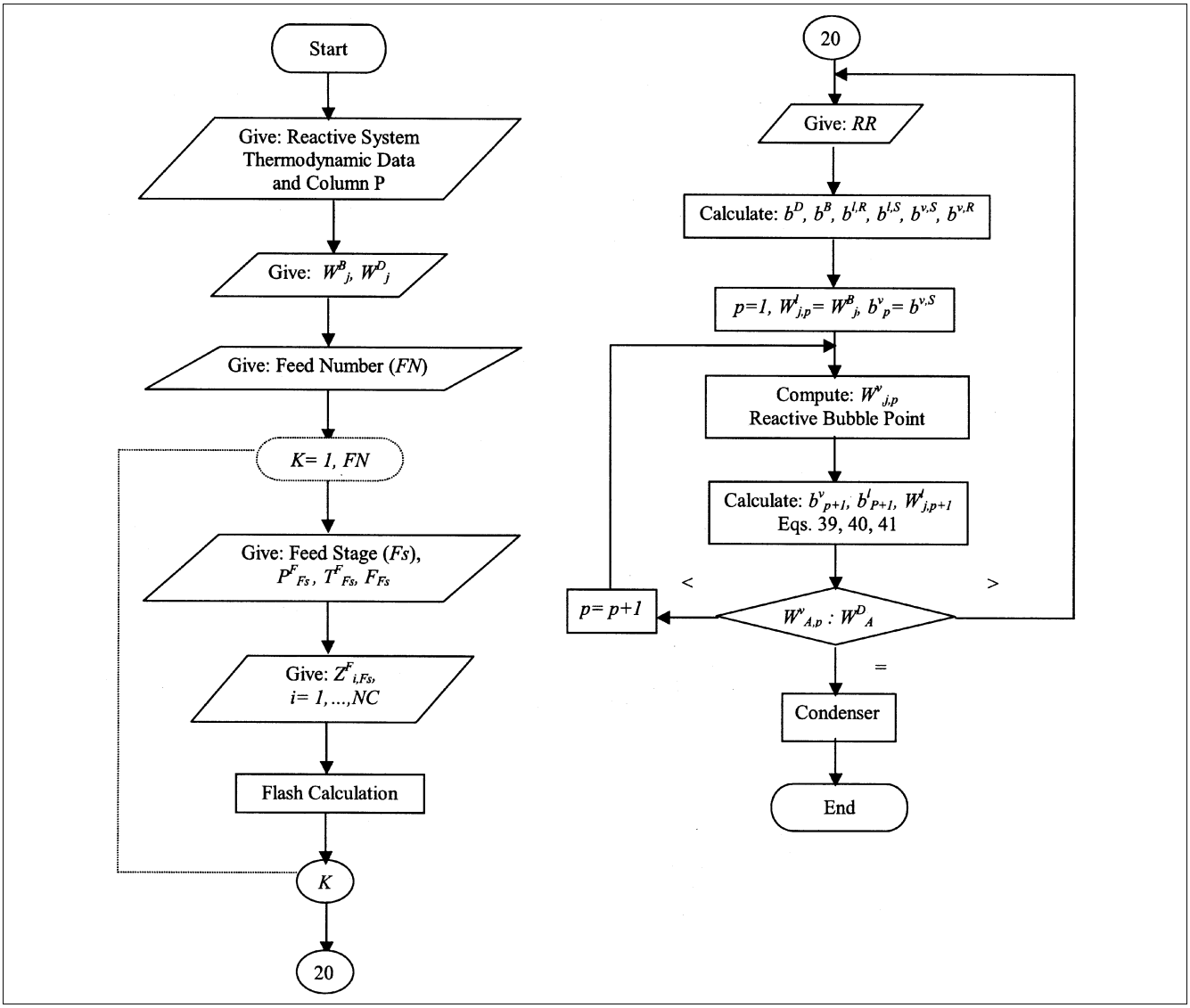

Figure 11. Algorithm 5: Reactive Lewis-Matheson method.

change in the liquid composition renders a vapor element composition, $W_A^v = 1.0$. Therefore, it is reasonable to state that the distillate product will contain pure formaldehyde.

For this reactive system the application of the reactive McCabe-Thiele method requires the following steps:

(1) Given operating pressure, compute the reactive equilibrium curve (see Figure 2);

(2) Give feed and product specifications (see Table 3);

(3) Obtain operating line intersection ($W_A^{l,I} = 0.58468$, $W_A^{v,I} = 0.78734$) from Eqs. 24 and 25;

(4) Draw reactive stages, starting from the bottom;

(5) Drawing successive reactive stages, if $W_A^v \cong W_A^D = 0.99$, then the final design has been obtained.

Table 8 gives detailed design results from the application of the reactive McCabe-Thiele method. From the reactive diagram it can be seen that six reactive stages are required to achieve the product specifications, and the feed should be located at stage 5, where the reactive operating lines intersect. With this design configuration, 5.34 moles of methylene glycol are produced.

Benzene production

The disproportionation of toluene to produce benzene and *o*-xylene, is an interesting equilibrium-limited reaction that could be improved through reactive distillation. Although benzene is now mostly produced through catalytic reforming (that is, toluene hydrodealkylation, pyrolysis of gasoline), in recent years, benzene production by toluene disproportionation has increased because of the growing demand for *p*-xylene (intermediate), and the differential cost of producing benzene from toluene sometimes becomes favorable. In the conventional reforming process, toluene or a mixture of toluene and C_9 aromatics are mixed with recycled hydrogen and heated from 350° to 530°C at 20–25 atm, and fed to a fixed-bed reactor with noble metal catalyst. The reaction is

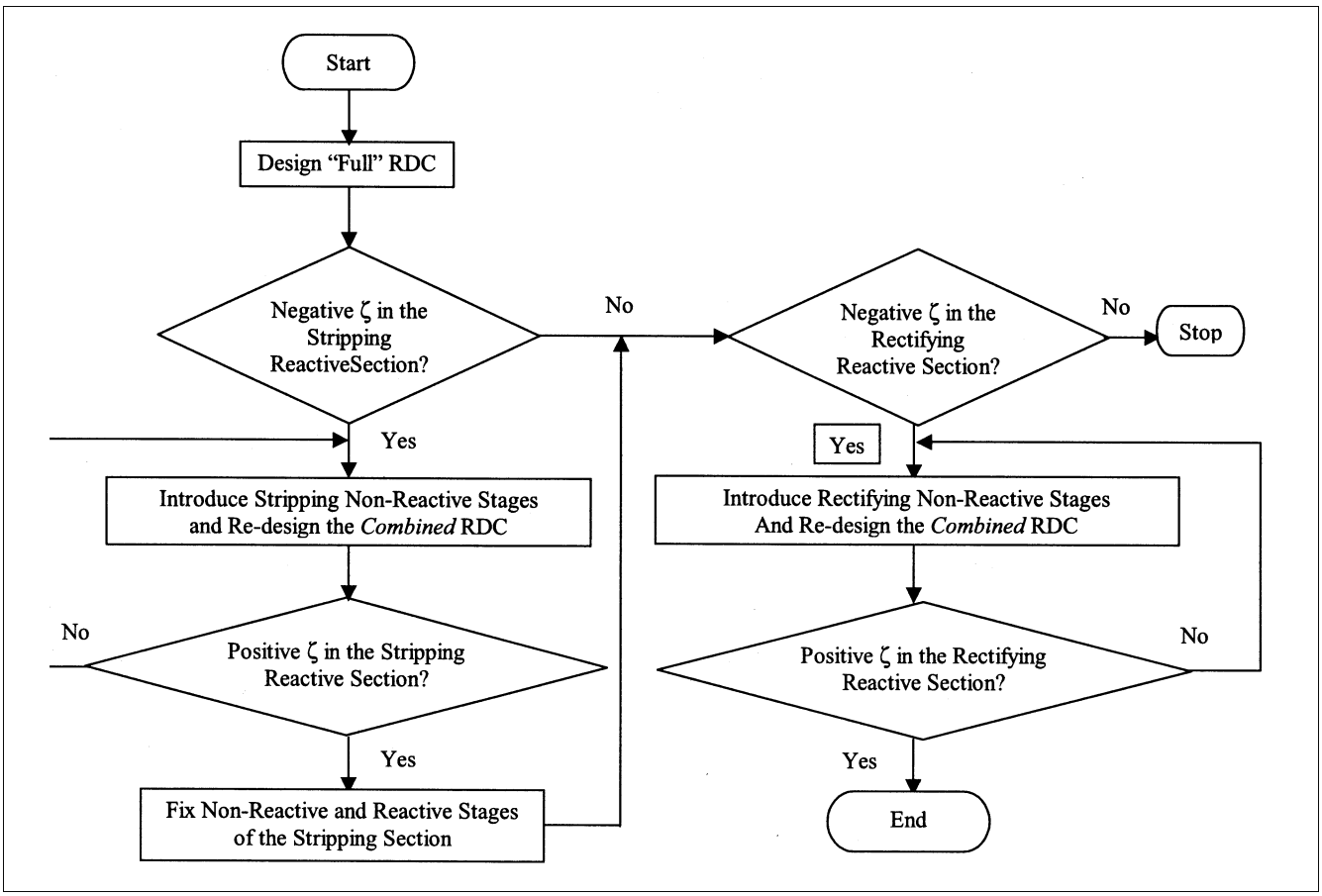

Figure 12. Algorithm 6: Combined reactive-distillation column design strategy.

Table 1. Reactive System 1: Methylene Glycol Production

CH_2O = Formaldehyde CH_4O_2 = Methylene Glycol $C_2H_6O_3$ = di-oxi-Methylene

$$CH_2O + H_2O \leftrightarrow CH_4O_2$$
$$2\,CH_4O_2 \leftrightarrow C_2H_6O_3 + H_2O$$

Element definition: $CH_2O = A$ $H_2O = B$

Element reactions: $A + B \leftrightarrow AB$

$$2\,AB \leftrightarrow B + B$$

	Formula Matrix			
	CH_2O (1)	H_2O (2)	CH_4O_2 (3)	$C_2H_6O_3$ (4)
A	1	0	1	2
B	0	1	1	1

Element fractions: $W_A^l = \dfrac{x_1 + x_3 + 2x_4}{x_1 + x_2 + 2x_3 + 3x_4}$ $W_B^l = \dfrac{x_2 + x_3 + x_4}{x_1 + x_2 + 2x_3 + 3x_4}$

Table 2. Reactive System 2: Benzene Production

$C_6H_6(CH_2)$ = Toluene C_6H_6 = Benzene $C_6H_6(CH_2)_2$ = *o*-xylene

$$2\,C_6H_6(CH_2) \leftrightarrow C_6H_6 + C_6H_6(CH_2)_2$$

Element definition: $C_6H_6 = A$ $(CH_2) = B$

Element reaction: $2\,AB \leftrightarrow A + AB_2$

	Formula Matrix		
	C_6H_6 (1)	$C_6H_6(CH_2)$ (2)	$C_6H_6(CH_2)_2$ (3)
A	1	1	1
B	0	1	2

Element Fractions: $W_A^l = \dfrac{x_1 + x_2 + x_3}{1 + x_2 + 2x_3}$ $W_B^l = \dfrac{x_2 + 2x_3}{1 + x_2 + 2x_3}$

Table 3. Reactive System 3a: MTBE Production (without inert)

Isobutene (C_4H_8) + Methanol (CH_4O) ↔ MTBE ($C_5H_{12}O$)
Element definition: $C_4H_8 = A$ $CH_4O = B$
Element reaction: $A + B \leftrightarrow AB$

Formula Matrix

	C_4H_8 (1)	CH_4O (2)	$C_5H_{12}O$ (3)
A	1	0	1
B	0	1	1

Element Fractions: $W_A^l = \dfrac{x_1 + x_3}{x_1 + x_2 + 2x_3}$ $W_B^l = \dfrac{x_2 + x_3}{x_1 + x_2 + 2x_3}$

Table 4. Reactive System 3b: MTBE Production (1-butene as inert)

Isobutene (C_4H_8) + Methanol (CH_4O) ↔ MTBE ($C_5H_{12}O$)
Element definition: $C_4H_8 = A$ $CH_4O = B$ 1-butene = C
Element reaction: $A + B \leftrightarrow AB$

Formula Matrix

	C_4H_8 (1)	CH_4O (2)	1-butene (3)	$C_5H_{12}O$ (4)
A	1	0	0	1
B	0	1	0	1
C	0	0	1	0

Element Fractions: $W_A^l = \dfrac{x_1 x_4}{x_1 + x_2 + x_3 + 2x_4}$

$W_B^l = \dfrac{x_2 + x_4}{x_1 + x_2 + x_3 + 2x_4}$

$W_C^l = \dfrac{x_3}{x_1 + x_2 + x_3 + 2x_4}$

Table 5. Reactive System 4: Ethanol Synthesis

C_2H_4 = Ethylene C_2H_6O = Ethanol $C_4H_{10}O$ = di-ethyl-ether
$C_2H_4 + H_2O \leftrightarrow C_2H_6O$
$C_2H_4 + C_2H_6O \leftrightarrow C_4H_{10}O$
Element definition: $C_2H_4 = A$ $H_2O = B$
Element reactions: $A + B \leftrightarrow AB$
$A + AB \leftrightarrow A_2B$

Formula Matrix

	C_2H_4 (1)	H_2O (2)	C_2H_6O (3)	$C_4H_{10}O$ (4)
A	1	0	1	2
B	0	1	1	1

Element fractions: $W_A^l = \dfrac{x_1 + x_3 + 2x_4}{x_1 + x_2 + 2x_3 + 3x_4}$

$W_B^l = \dfrac{x_2 + x_3 + x_4}{x_1 + x_2 + 2x_3 + 3x_4}$

carried out in the vapor phase. Since disproportionation of toluene is an equilibrium reaction, the ratio of xylene to benzene can be changed by varying the feedstock and operating conditions. Stitt (2002) has performed an economic evaluation of a reactive distillation process for this reactive system based on a numerical simulation in Aspen Plus, and concludes that the reaction does not prove to be a fruitful development opportunity for reactive distillation due to economic considerations. Despite this conclusion, the characteristics of the reactive system still have an academic importance for the development of design procedures.

For this reactive system, the thermochemical and vapor pressure data were taken from the Aspen DIPPR data bank. The vapor phase is considered an ideal gas, and the NRTL model was used to calculate the activity coefficients of the liquid phase. The element representation of the reactive system is given in Table 2. Note that for this reactive element system, the element B is "CH2," which is not a whole molecule and, therefore, cannot exist by itself. Therefore, since it is associated with the less volatile compounds (toluene and *o*-xylene), it is regarded as a less volatile element. Also for this reason, the element B is not the only one considered in the plotting of the phase diagrams, while AB_2 (or AB) is used. Note also that the reaction zone is only located for $0.33 < W_A^L < 1$. The feed and product specifications, and the operation pressure, are given in Table 7. The objective in the design of this reactive-distillation column is to obtain high-purity benzene at the top of the column and a mixture of toluene and *o*-xylene at the bottom.

Figure 4 shows the reactive equilibrium curve and the operating lines employed for the configuration of a full reactive distillation column for the production of benzene based on a reactive McCabe-Thiele diagram using Algorithm 2 in Figure 6. Twelve reactive stages are required to produce 40.34 moles of high-purity benzene, and the feed must be located at stage 5 for a reflux ratio of 7.51. A reactive Ponchon-Savarit diagram for this system was constructed (see Figure 7) using Algorithm 3 in Figure 9. The application of the Ponchon-Savarit method to this reactive system requires the following steps:

(1) Given operating pressure, compute the reactive equilibrium curves $H_{CPE}^{b,v}$ and $H_{CPE}^{b,l}$;

(2) Give feed and product specifications (see Table 7);

Table 6. Resulting Designs from the Proposed Design Algorithms*

System	Design Algorithm	Total Stages**	Feed Stage	RR	Bottom Product (mol)
1	Reactive McCabe-Thiele	7	5	1.00	39.7944
2	Reactive McCabe-Thiele	13	5	7.51	59.5041
2	Reactive Ponchon-Savarit	12	4	6.30	59.5041
3a	Reactive McCabe-Thiele	6	3	2.12	31.0836
3a	Reactive Ponchon-Savarit	6	3	1.75	31.0836
3b	Reactive Lewis-Matheson	10	7	3.49	38.7325
4	Reactive driving force	9	4	2.50	39.3450

*Feed composition and quality as in Table 7.
**Nonreactive total condenser included.

Table 7. Full RDC Design Specifications

System	P (kPa)	$\theta^{F,v}$	Vapor Phase	Liquid Phase
1	101.3	0.14742	Ideal gas	UNIFAC model
2	101.3	0	Ideal gas	NRTL model
3a	101.3	0.7590	SRK equation	Wilson model
3b	1100	0.666	Ideal gas	NRTL model
4	3546.4	0.05	Ideal gas	NRTL model

System	Element	W^F	W^B	W^D	Component	z^F	x^B	y^D
1	*A*	0.6	0.2	0.99	Formaldehyde	0.6	0.007557	0.989836
	B	0.4	0.8	0.01	Water	0.4	0.805162	0.000002
					Methylene G	0	0.134008	0.003954
					Poly(oxym) G	0	0.053273	0.006208
2	*A*	0.5	0.375	0.98	Benzene	0	0.010322	0.979624
	B	0.5	0.625	0.02	Toluene	1.0	0.312690	0.020344
					o-Xylene	0	0.676988	0.000032
3.a	*A*	0.7	0.5	0.994	Isobutene	0.7	0.042677	0.993964
	B	0.3	0.5	0.006	Methanol	0.3	0.042677	0
					MTBE	0	0.914647	0.006036
3.b	*A*	0.35	0.463	0.149998	Isobutene	0.35	0.114098	0.135571
	B	0.332764	0.511229	0.016894	Methanol	0.332764	0.193662	0.000208
	C	0.317236	0.025771	0.833108	1-Butene	0.317236	0.042515	0.847248
					MTBE	0	0.649725	0.016973
4	*A*	0.65	0.6066	0.8268	Ethylene	0.65	0.097	0.745
	B	0.35	0.3934	0.1732	Water	0.35	0.071	0.015
					Ethanol		0.369	0.005
					Di-EthylEther		0.464	0.235

(3) Calculate $H^{b,D}$, $H^{b,N}$, ΔD, $H^{b,F}$, ΔB, $H^{b,B}$ and build the operating lines;

(4) Draw reactive stages starting from the bottom;

(5) Drawing successive reactive stages, if $W_A^v \cong W_A^D = 0.98$, then the final design has been obtained.

Table 9 gives the detailed design results of the Ponchon-Savarit method (Algorithm 3 in Figure 9). It can be noted in Figure 9 that by considering the heat effects, one reactive stage is eliminated, the reflux ratio was reduced to 6.30, and the feed location is at stage 4. However, the product composition specifications were the same as those for the design obtained with the reactive McCabe-Thiele method. Numerical simulations using Aspen Plus were performed where the results from the reactive McCabe-Thiele method were used to specify the column parameters. Figure 13 shows the temperature profile along the reactive distillation column, and it can be observed that the maximum temperature difference between the simple design and simulation results (that is, 10 degrees) occurs at stage 7. Figure 14 shows the benzene generation profile along the column. It can be noted that the production of benzene occurs mainly at the feed stage. The difference in benzene generation between the simple design and the rigorous simulation are not too great, and the rigorous profiles from the simple design serve as very good initial

Table 8. McCabe-Thiele Method Results: Algorithm 2

Reactive System 1 Equilibrium Stages		
Stage	W_A^l	W_A^v
Points over CPE curve	Values from operating lines Eqs. 22, 23	Reactive Bubble-point calculation
Reboiler	0.2	0.31295
2	0.27398	0.42591
3	0.34796	0.54749
4	0.42759	0.68990
5	0.52087	0.86036
6	0.73072	0.99515
Condenser	0.99515	
	Operating line $W_A^{l,I}$	**Intersection** $W_A^{v,I}$
	From Eq. 24	From Eq. 25
	0.58468	0.78734

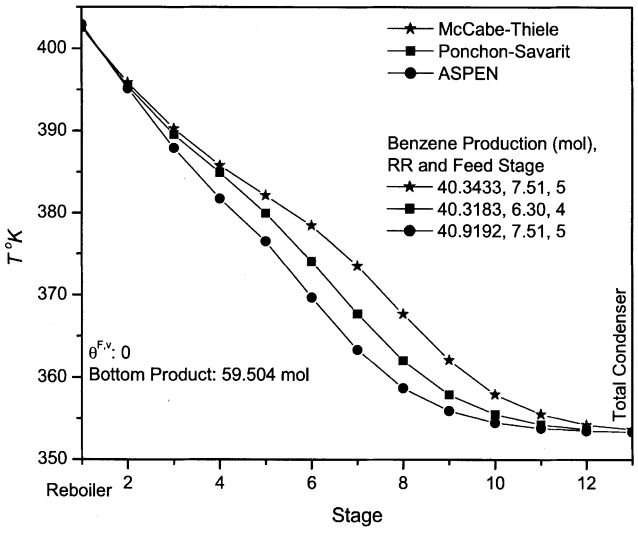

Figure 13. Temperature profile comparison: reactive system 2 (isenthalpic reaction).

Table 9. Ponchon-Savarit Method Results: Algorithm 3

Element Composition	Reactive System 2 Operating Lines Element Enthalpy (J/mol)	From Equation
$W_A^D = 0.98$	$H^{b,D} = 55318.26$	17
$W_A^D = 0.98$	$H^{b,N} = 85547.75$	18
$W_A^D = 0.98$	$\Delta D = 275993.64$	35
$W_A^F = 0.50$	$H^{b,F} = 26446.58$	17
$W_A^B = 0.375$	$\Delta B = -38539.63$	34
$W_A^B = 0.375$	$H^{b,B} = 3198.5$	17

	Equilibrium Stages			
Stage	W_A^l Eqs. 30, 27 for Stripping Sec. Eqs. 28, 27 for Rectifying Sec.	$H^{b,l}$ From Eq. 17 (J/mol)	W_A^v Reactive Bubble-Point Calculation	$H^{b,v}$ From Eq. 18 (J/mol)
	—	—		
Reboiler	0.37500	3198.50	0.4146	21408.64
2	0.40406	5449.52	0.45845	26212.06
3	0.43489	7927.67	0.50086	30912.72
4	0.46346	10276.23	0.53954	35251.54
5	0.49934	13277.69	0.58879	40829.97
6	0.55014	17594.99	0.65794	48722.75
7	0.62270	23853.54	0.74679	58901.59
8	0.71808	32182.30	0.83883	69451.77
9	0.81946	41107.67	0.91131	77751.06
10	0.90111	48327.82	0.95639	82908.09
11	0.95272	52899.54	0.98041	85654.45
Condenser	0.98041	85654.45		

estimates for the rigorous simulation (thereby making the rigorous simulation more efficient).

However, a careful analysis of this profile leads to the realization that the designed reactive distillation column is not necessarily the optimum design. As can be observed in Figure 14, the generation of benzene is negligible from the reactive stage 8 to the top, while the opposite is true from stages 2 to 6; thus, the reactive distillation column is overdesigned in terms of the number of reactive stages used. Therefore, the design of a combined reactive distillation column proceeds. Using Algorithm 6 (as described in the "Design Strategy" section and in Figure 12), a combined reactive distillation column for producing high-purity benzene was designed. Table 10 gives the results of such a design in terms of the generation of benzene and temperature at each stage. It can be noted that there are stages with zero generation, which means that a nonreactive stage has been considered.

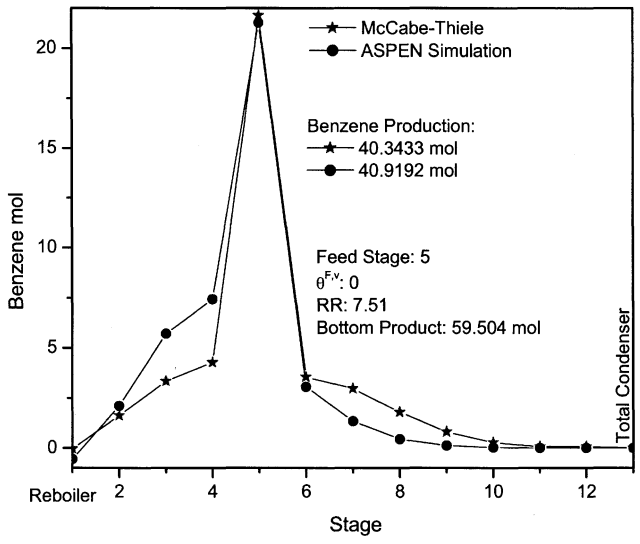

Figure 14. Product-generation profile comparison: reactive system 2.

Table 10. Combined RDC Design*

	Step 1. "Full" RDC (Figure 4) From Algorithm 2		Step 3. Final Design	
Stage	Benzene Production	T (K)	Benzene Production	T (K)
1	−0.043500	402.5092	0	402.886443
2	1.613234	395.8566	1.59338837	395.089813
3	3.333685	390.2865	5.73802812	387.876925
4	4.282890	385.7979	7.43571605	381.698416
5	21.633039	382.1133	21.2336135	376.502611
6	3.549146	378.4454	3.04205021	369.675664
7	2.966896	373.5454	1.33019949	363.341706
8	1.794092	367.7159	0.43763018	358.684872
9	0.803806	362.1059	0.14386368	355.920587
10	0.268949	357.9546	0	354.499059
11	0.067933	355.5046	0	353.822071
12	0.073169	354.2555	0	353.510717
13	0	353.6695	0	353.370108
Total moles	40.343340		40.95440000	

*Reactive system 2: Algorithm 6.

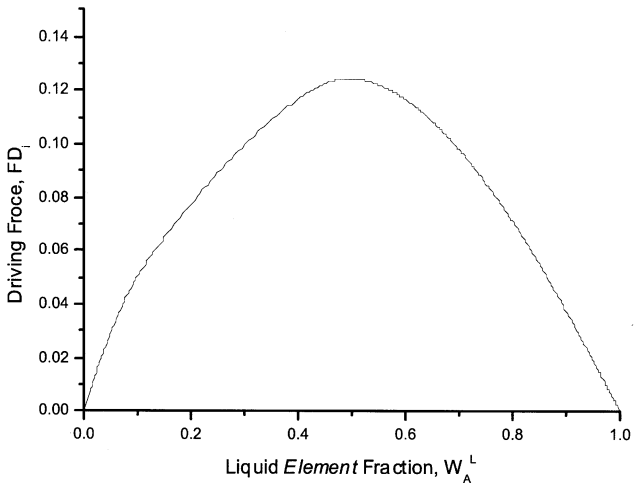

Figure 15. Reactive driving-force diagram (normalized element fractions): reactive system 2.

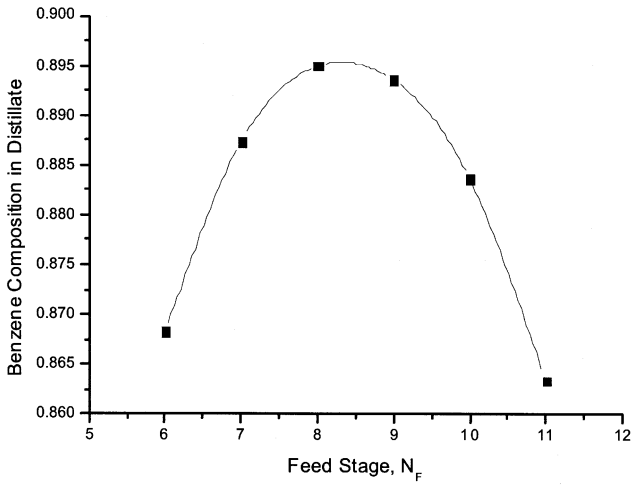

Figure 16. Benzene purity for different feed locations.
Reactive driving-force approach. Reactive system 2.

Finally, the reactive driving-force approach was used to design an energy-efficient reactive distillation column for this reactive system. Figure 15 shows the rescaled reactive driving-force diagram. Based on this diagram, the change of the feed location was proposed, as described by Algorithm 4 (Figure 10). Going through the driving-force design procedure in Algorithm 4, the following steps are performed. From Figure 4 we get the binary-element vapor–liquid equilibrium data. From these data, we obtain the driving-force diagram, which is given in Figure 15 with rescaled axis. The feed conditions are given in Table 7, and it is noted that the feed is vaporized. N_F is determined by calculating $N_F = (1 - D_x)\, N_P$, but in this case, D_x is the point of the vaporized feed. This point is found by adding the horizontal distance on the composition axis corresponding to the size of the vapor-phase equilibrium step in the vapor–liquid diagram to the "normal" point of the largest driving force, D_x. This is indicated in Figure 15. The minimum reflux ratio is found to be 3.1 (element based), and the desired products are pure benzene in the distillate product and toluene/*o*-xylene in the bottom product at a ratio of 2 to 1. It can be observed in Figure 16 that moving the feed location and maintaining the heat duty in the reboiler constant, the benzene purity passes through a maximum value, clearly indicating the optimum-stage location of the feed. In this case, it was decided to keep the heat duty constant because the reactive system behaves as an isenthalpic system, as was pointed out by Stitt (2002) and the temperatures of vaporization for the different compounds are very similar. The actual reflux ratio in this case is 5.3. This approach, however, is, in this case, slightly different from the proposed method, due to the isenthalpic behavior of this system. Nevertheless, considering that the feed in this system is vapor, it can be noted that the optimum feed-stage location matches the prediction of Algorithm 4 (see Figure 10).

MTBE production

The production of MTBE from the reaction of isobutene with methanol in the presence of inert components (*n*-butane and/or 1-butene) is an important process because of the characteristics of MTBE as an antiknock agent (Smith, 1982). This system has been studied extensively by Doherty and coworkers (Barbosa and Doherty, 1987; Doherty and Buzad, 1992; Ung and Doherty, 1995). Distillation simulation studies are also reported by Jacobs and Krishna (1993), Hauan et al. (1995), Abufares and Douglas (1995), Pérez-Cisneros et al. (1996), Alejski and Duprat (1996), and Pilavachi et al. (1997). For system 3a the computation of the chemical and physical equilibrium is based on the thermochemical data of Rehfinger and Hoffmann (1990) as reported by Zhang and Datta (1995), with the Antoine constants for the vapor pressure given by Ung and Doherty (1995), and the Wilson model for calculating the activity coefficients and the SRK equation of state for the vapor phase are used. For system 3b the liquid and vapor-phase behavior was represented by NRTL and ideal models, respectively, and the necessary information was taken from the DIPPR data bank. The element representation of the reactive system is given in Tables 3 and 4.

The design of reactive distillation columns for the production of MTBE, involves a binary-element system (without an inert component) and a ternary-element system (1-butene as the inert component). The reactive McCabe-Thiele and Ponchon-Savarit diagrams have been used for the binary-element case. For the ternary-element case and the combined RDC, the reactive Lewis-Matheson method is used. Numerical simulations have been performed in order to validate the reactive-distillation column design.

MTBE production without inert component

When the inert component is not considered, the MTBE reactive system can be represented by only two elements, and a quick design for a full RDC through the reactive McCabe-Thiele diagram can be performed. The feed and product specifications are given in Table 7. Figure 17 shows the results for a reactive distillation column design at $P = 1$ atm. Following the design method, it can be noted that four reactive stages plus a partial reboiler (reactive stage) and the feed placed at stage 3 are required to achieve the output specifications. Figure 8 shows the results using a reactive Ponchon-

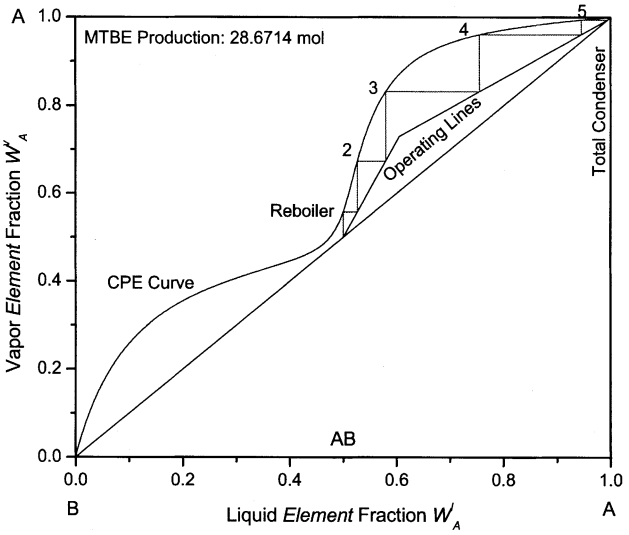

Figure 17. Reactive element McCabe-Thiele diagram: reactive system 3a.

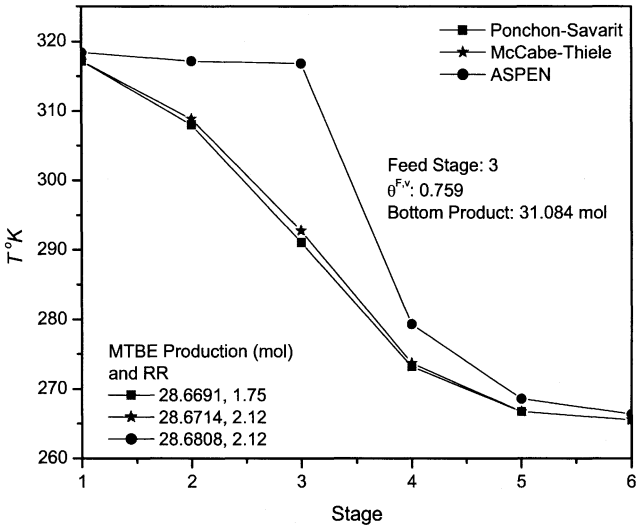

Figure 18. Temperature profile comparison: reactive system 3a (exothermic reaction).

Savarit diagram. It can be noted in Figure 8 that, by taking the heat effects into consideration, there is no difference in the number of reactive stages required. However, to achieve the product composition specifications, a lower reflux ratio of 1.75 should be used. This result can be explained as follows: when the heat effects are considered, the heat of reaction becomes important and, in this case, it is an exothermic reaction. This can be seen more clearly by comparing the temperature profiles (see Figure 18) obtained through rigorous simulation and the simple design obtained using the reactive McCabe-Thiele diagram. Aspen Plus simulation gives a higher temperature profile than the simple design, since a rigorous simulation considers the energy balances, and in this case the reaction considered is exothermic.

Taking the design results as the initial values for the temperature and composition profiles, the simulation required only 5 iterations to obtain convergence, while 13 iterations are required without the supplied estimates. Thus, the design tools not only gave reasonable design estimates but improved the simulation efficiency by providing "good" estimates of the temperature and composition profiles.

Figure 19 shows the generation profiles for MTBE along the reactive-distillation column. The larger differences in MTBE generation occur at stages 3 and 4, where there is a wide temperature difference, too. From Figure 19 it can be noted that there are some reactive stages with negative generation (stages 1 and 5), that is, decomposition of MTBE occurs, and a combined reactive distillation column is proposed. Table 11 gives the results for the design of a combined

Table 11. Combined RDC Design Strategy*

	Step 1. "Full" RDC (Figure 17) From Algorithm 2		Step 2. Two Nonreactive Stages in Bottom Adjusted	
Stage	MTBE Production	T (K)	MTBE Production	T (K)
1	−3.23119	317.1394	0	321.7722
2	1.48982	308.8676	0	310.1880
3	30.3363	292.7079	27.404162	293.1612
4	0.07666	273.6968	0.079422	275.8406
5	−1.52E-4	266.7470	2.768375	268.0441
6	0	265.5593	0	265.6958
Total moles	28.67144		30.251959	
	Step 3. Final Design		ASPEN Simulation	
Stage	MTBE Production	T (K)	MTBE Production	T (K)
1	0	321.7722	0	321.240482
2	0	310.1880	0	318.289418
3	27.404162	293.1612	20.7895644	317.059873
4	2.617918	275.8406	8.28102623	279.488229
5	0	267.1903	0	268.652297
6	0	265.6024	0	266.369555
Total moles	30.022080		29.07059063	

*Reactive system 3a: Algorithm 6.

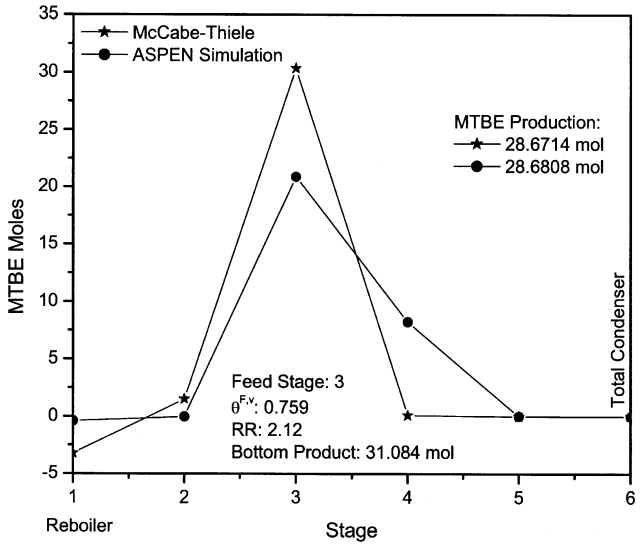

Figure 19. Product-generation profile comparison: reactive system 3a.

reactive-distillation column following the three steps given in the "Design Strategy" section.

The equivalent driving-force diagram is calculated, and is plotted in Figure 5. Note that the bottom composition in the phase diagram for the reaction zone is approximately 0.5, which corresponds to pure MTBE on a compound basis, and therefore a high-purity MTBE product can be achieved, because the reactants contribute equally to the reaction. The procedure for determining the operating conditions is applied, as described in the "Reactive Driving-Force Approach" section. The feed composition specifications and the operating pressure of the column are similar to the McCabe-Thiele design, but with a feed vaporization fraction of 0.83.

The driving-force diagram with the relevant points is given in Figure 5a. Clearly, the objective of this reactive column is

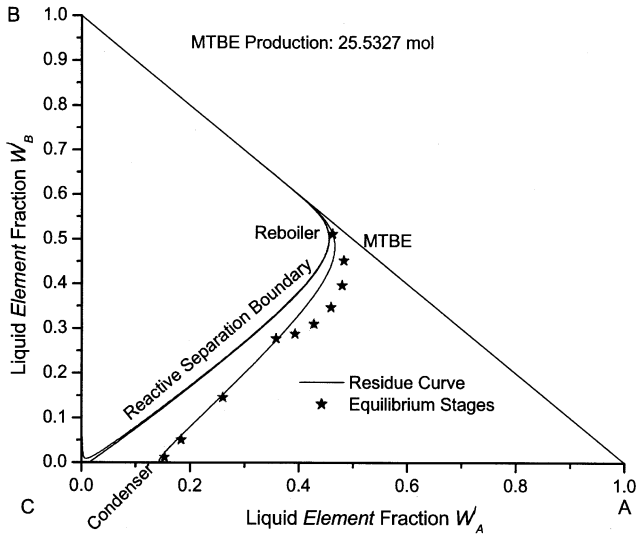

Figure 20. Reactive element ternary diagram.

Lewis-Matheson method. Reactive system 3b.

Table 12. Lewis-Matheson Method Results: Algorithm 5

Reactive System 3b From Reactive Bubble-Point Calculation			
Stage	W_A^v	W_B^v	W_C^v
1	0.49759302	0.41157387	0.09083310
2	0.49205025	0.31970731	0.18824244
3	0.45737629	0.23793435	0.30468936
4	0.40509141	0.17697047	0.41793812
5	0.34654904	0.14043693	0.51301403
6	0.28862786	0.12281699	0.58855515
7	0.23448547	0.11683105	0.64868348
8	0.17400974	0.04263234	0.78335792
9	0.15031576	0.01182520	0.83785904
10	0.15031576	0.01182520	0.83785904
From Eqs. 39–41			
Stage	W_A^l	W_B^l	W_C^l
1	0.46300000	0.51122900	0.02577100
2	0.48371478	0.45155414	0.06473108
3	0.48039569	0.39654318	0.12306114
4	0.45963244	0.34757640	0.19279116
5	0.42832354	0.31107039	0.26060607
6	0.39326756	0.28919360	0.31753884
7	0.35858356	0.27864254	0.36277390
8	0.25869384	0.14546630	0.59583987
9	0.18088983	0.05000722	0.76910295
10	0.15031576	0.01182520	0.83785904

to produce MTBE as the bottom product and in the top isobutene. For verification purposes, rigorous simulations were performed in Aspen Plus. The column specifications given for the rigorous simulation are the reflux ratio (molar basis) = 2.5, and recovery of methanol and MTBE at the bottom (0.997). The results of the calculations are shown in Figure 5b. It is clearly verified that, from an energy point of view, and with consistent column specifications, the actual optimum feed stage matches the prediction.

MTBE production with inert component

When an inert component (1-butene and/or *n*-butane) is considered, the MTBE reactive system is represented by three elements. A reactive Lewis-Matheson method for design of reactive distillation columns (as is described in the "Ternary-Element Reactive Systems" section and Algorithm 5 in Figure 11) can be used. The input and output specifications are given in Table 2. Figure 20 shows the full reactive-distillation column design configuration obtained through the application of the reactive Lewis-Matheson method. Detailed design results can be seen in Table 12. It can be observed in Figure 20 that nine reactive stages plus a total condenser are required to achieve the product specifications, and that the feed is located at stage 7. Figures 21 and 22 show the temperature and generation profiles, respectively. As in the noninert case, the temperature and generation differences are because the rigorous simulation accounts for the heat effects. Table 13 gives the results for the design of a combined reactive-distillation column, and four nonreactive stages at the stripping section are introduced. Taking the design results as initial values for the temperature and composition profiles, the rigorous simulation in Aspen Plus required only nine iterations to obtain convergence, while 15 iterations are required without the supplied estimates. It should be noted here that since

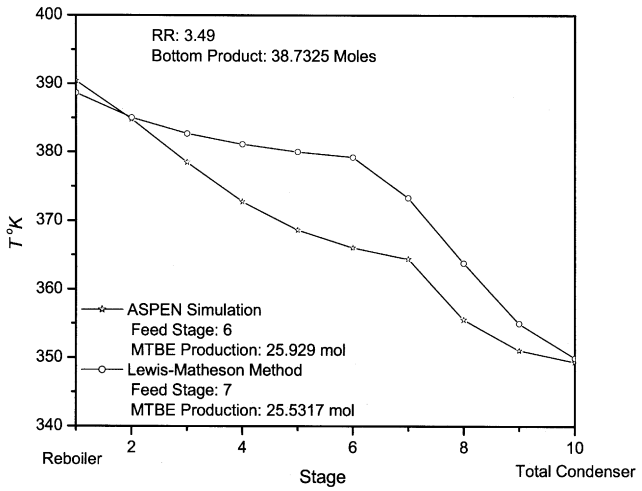

Figure 21. Temperature profile comparison: reactive system 3b (exothermic reaction).

there were differences in the databases and property model parameters between CPE/ICAS and Aspen Plus, the transfer of initial estimates included some differences between the property values from the two data sources. Therefore, the reduction in the number of iterations is only about 50%. If the same data source is used (checked independently within ICAS for a nonreactive system), the reduction is nearly 90%.

Ethanol synthesis

This example concerns the synthesis of ethanol from ethylene and water. The reaction scheme and the element representation for this reactive system is given in Table 5. This reactive system could be considered more complicated, because there are two simultaneous reactions taking place and because of the phase behavior. Note, however, that still only two elements are needed to represent the reactive system.

The reactive distillation process is taking place at $P = 35$ atm. The phase behavior is described by the NRTL model

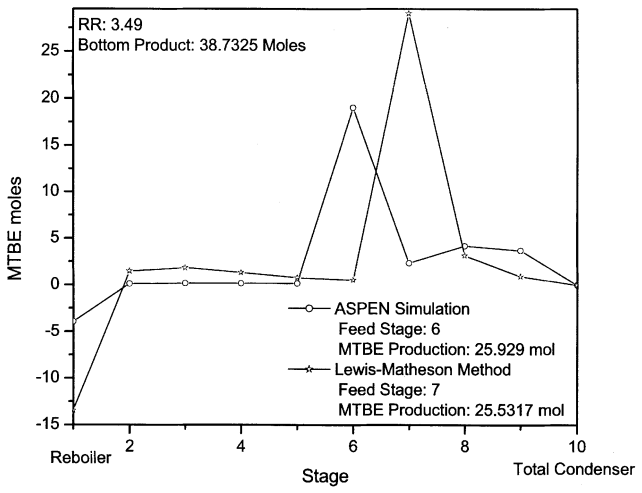

Figure 22. Product-generation profile comparison: reactive system 3b.

Table 13. Combined RDC Design*

Stage	Step 1. "Full" RDC (Figure 20) From Algorithm 5 MTBE Production	T (K)	Step 3. Final Design MTBE Production	T (K)
1	−13.445546	390.4128	0	391.556398
2	1.462636	384.7758	0	382.966908
3	1.822818	378.4776	0	380.345839
4	1.341243	372.7426	0	379.595145
5	0.783180	368.5845	0	379.375735
6	0.511002	366.0022	18.908586	379.307948
7	29.026457	364.3922	2.06636517	373.503430
8	3.133769	355.5301	3.83148822	364.051106
9	0.896206	351.0343	3.66593922	355.192269
10	0.000000	349.3776	0	349.939944
Total moles	25.53176		28.473	

*Reactive system 3b: Algorithm 6.

and ideal gas. Note that the selection of ideal gas for the vapor phase is based on an arbitrary assumption, as ethylene is a supercritical compound under the given operating conditions. In this case, the reactive driving-force approach has been applied to obtain an energy-efficient design of the reactive distillation column. The total column has nine stages, including reboiler and condenser. The three top stages (except the condenser) are reactive. The feed is a mixture of ethylene and water, which enters at the reactive zone, and by using Algorithm 4 (Figure 10), it was found that the optimum feed location is at stage 4. Unreacted ethylene enters the top of the column, and the water/ethanol mixture enters the bottom, together with a small amount of diethyl ether. Below the reactive zone there is a stripping zone for the concentration of ethanol. Figure 23 shows the element reactive phase diagram and Figures 24 and 25 show the driving-force diagrams. It can be seen clearly from the reactive phase diagram that ethylene could be distilled in a reasonably pure format at the top of the column. However, in the bottom of the reactive zone there is a mixture of water, ethanol, and diethyl ether. In order to concentrate the water and minimize the diethyl ether, an additional stripping section is added below the reaction zone. To verify the design, rigorous simulations were carried out in Aspen Plus. The column specifications are: reflux ratio (molar basis) = 2.5, and the reboiler duty was varied to match the ethanol composition at the bottom (0.369). It is clear, from Figure 26 that the minimum reboiler duty obtained through rigorous simulation occurs when the feed is located at stage 4, corresponding to the feed location predicted using the reactive driving-force approach.

Conclusions

Four methods for designing an RDC have been developed. Based on the element mass-balance concept, three graphical methods for binary-element reactive systems are used for designing distillation columns comprising only reactive stages, that is, full reactive-distillation columns. The driving-force approach of Gani and Bek-Pedersen (2000) to obtain energy-efficient designs has been extended to include reactive systems. The reactive driving-force approach appears to be an excellent procedure to indicate how and which operating variables could be manipulated in order to obtain an en-

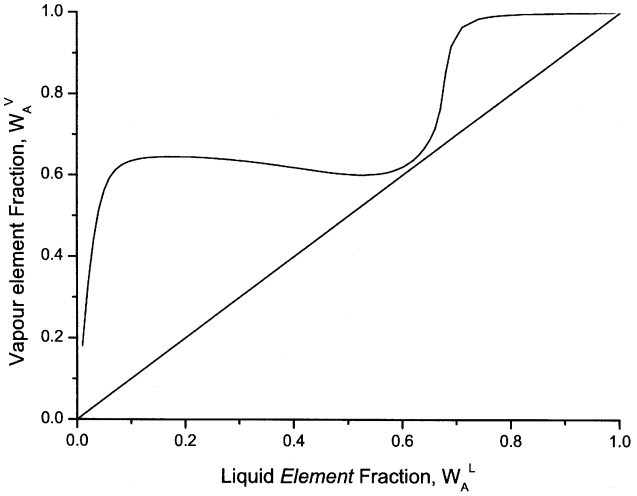

Figure 23. Reactive phase diagram for ethanol synthesis: reactive system 4.

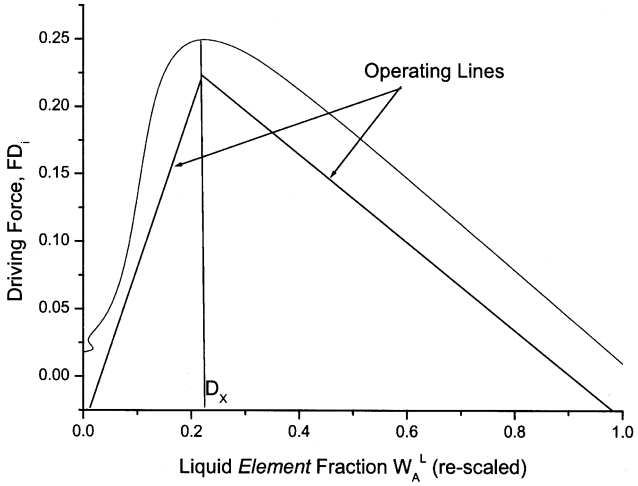

Figure 25. Reactive driving-force diagram: reactive system 4 (rescaled).

ergy-efficient design of a reactive-distillation column. When the number of elements is greater than two, or when a combined configuration of an RDC is considered, the stage-to-stage calculation method (reactive Lewis-Matheson) is used. In the examples presented here, a strategy for designing a combined RDC was developed that included the tracking of the generation and temperature at each reactive stage. This strategy required the use of reactive and nonreactive bubble-point calculations. The final designs obtained have been verified through rigorous simulations, and the difference between the results obtained with the basic design methods and the simulation results were not very large. Considering the speed and simplicity of the simple calculations, the results from the developed methods serve as useful first estimates of the design problem. In addition, the simple design methods generate estimates of composition and temperature profiles, which when included in the rigorous simulation model, significantly increase its convergence efficiency. Therefore, the proposed simple design methods serve to provide quick and reliable designs as well as to provide very good starting points for rigorous simulation models. Finally, since well-known concepts from the design of nonreactive distillation columns are used, once the transformation to elements is made for the reactive systems, the design methods for reactive and nonreactive systems are the same and easy to visualize. While the element concept is shown to be very powerful in designing reactive-distillation columns for two- or three-element reactive systems (multicomponent reactive systems with more than three compounds), some difficulties were encountered when it was applied to electrochemical reactions where charge balances must be incorporated the identification of the corresponding elements is not a simple task. Also, as with most visual methods, the visual algorithms of the element-based approach can only be used if two or three elements represent the reactive system. Otherwise, the nonvisual algorithms (reactive Lewis-Matheson) need to be used.

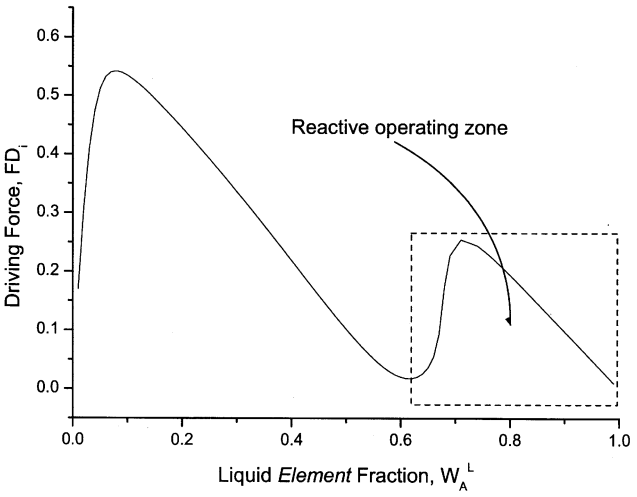

Figure 24. Reactive driving-force diagram: reactive system 4.

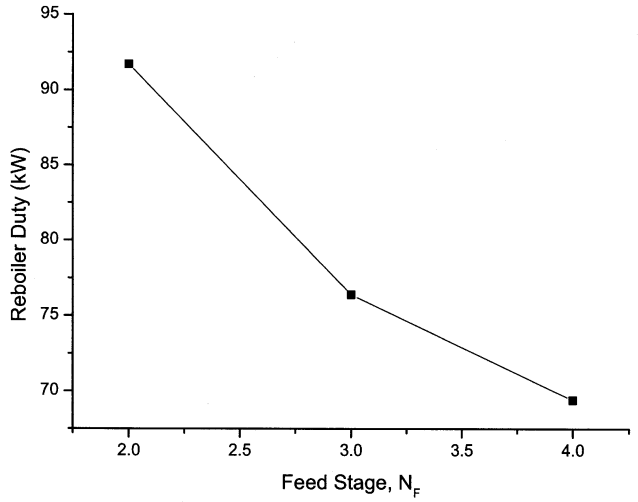

Figure 26. Reboiler heat duty as function of the feed-stage location.

Rigorous simulation. Reactive system 4.

Notation

A^b = formula matrix
b^F = total feed flow (*element* based)
b^B = total bottom-product flow (*element* based)
b^D = total distillate-product flow (*element* based)
b^l = liquid element stream
b^v = vapor element *stream*
A, B, C = elements
F_{Di} = component-based driving force
F_{Di}^b = *element*-based driving force
$H^{b,l}$ = liquid enthalpy stream (*element* based)
$H^{b,v}$ = vapor enthalpy stream (*element* based)
$H^{b,B}$ = bottom-product enthalpy (*element* based)
$H^{b,D}$ = distillate product enthalpy (*element* based)
$H^{b,F}$ = feed enthalpy (*element* based)
L = liquid stream (*component* based)
M = total number of elements in the system
NC = total number of components in the system
N = total number of plates
P = pressure
$q^{b,B}$ = reboiler duty (*element* based)
$q^{b,D}$ = condenser duty (*element* based)
R = rectifying section
S = stripping section
T = temperature
T^F = feed temperature
V = vapor stream (*component* based)
W^l = liquid element fraction
W^v = vapor element fraction
W^B = element fraction in the bottom product
W^D = element fraction in the distillate product
W^F = element fraction in the feed
x = liquid mole fraction
x^B = mole fraction in bottom product
x^D = mole fraction in distillate product
y = vapor mole fraction
z^F = feed mole fraction

Greek letters

α_{ij} = relative volatility
α_{ij}^b = element relative volatility

Literature Cited

Abufares, A. A., and P. L. Douglas, "Mathematical Modelling and Simulation of an MTBE Catalytic Distillation Process Using SPEEDUP and ASPENPLUS," *Trans. Inst. Chem. Eng.*, **73A**, 3 (1995).

Agreda, V. H., L. R. Partin, and W. H. Heise, "High-Purity Methyl Acetate via Reactive Distillation," *Chem. Eng. Prog.*, **86**, 40 (1990).

Albert, M., I. Hahnenstein, H. Hasse, and G. Maurer, "Vapor-Liquid Equilibrium of Formaldehyde Mixtures: New Data and Model Revision," *AIChE J.*, **42**(6), 1741 (1996).

Alejski, K., and F. Duprat, "Dynamic Simulation of the Multicomponent Reactive Distillation," *Chem. Eng. Sci.*, **51**, 4237 (1996).

Barbosa, D., and M. F. Doherty, "Design of Multicomponent Reactive Distillation Columns," *Chem. Eng. Symp. Ser.*, **194**, B369 (1988).

Bessling, B., G. Schembecker, and K. H. Simmrock, "Design of Processes with Reactive Distillation Line Diagrams," *Ind. Eng. Chem. Res.*, **36**, 3032 (1997).

Brandani, V., and G. DiGiacomo, "Thermodynamic Consistency of Vapor-Liquid Equilibrium Data for the Water-Formaldehyde System," *Ind. Eng. Chem. Fundam.*, **23**, 126 (1984).

Doherty, M. F., and G. Buzad, "Reactive Distillation by Design," *Trans. Inst. Chem. Eng.*, **70A**, 448 (1992).

Chaddha, N., M. F. Malone, and M. F. Doherty, "Effect of Chemical Kinetics on Feasible Splits in Reactive Distillation," *AIChE J.*, **47** (3), 590 (2001).

Espinosa, J., N. Scenna, and G. Perez, "Graphical Procedure for Reactive Distillation Systems," *Chem. Eng. Commun.*, **119**, 109 (1993).

Espinosa, J., P. Aguirre, and G. Perez, "Some Aspects in the Design of Multicomponent Reactive Distillation Columns Including Non-reactive Species," *Chem. Eng. Sci.*, **20**, 469 (1995).

Espinosa, J., P. Aguirre, and G. Perez, "Some Aspects in the Design of Multicomponent Reactive Distillation Columns—Columns with a Reactive Core—Mixtures Containing Inerts," *Ind. Eng. Chem. Res.*, **35**, 4437 (1996).

Gani, R., and E. Bek-Pedersen, "Simple Algorithm for Distillation Column Design," *AIChE J.*, **46**(6), 1271 (2000).

Gani, R., M. Hostrup, J. W. Kang, J. Marrero, and M. R. Eden, *ICAS — Documentations*, CAPEC Rep. PEC02-23, Technical Univ. of Denmark, Lyngby, Denmark (2002).

Gumus, Z. H., and A. R. Ciric, "Reactive Distillation Column Design with Vapor/Liquid/Liquid Equilibria," *Comput. Chem. Eng.*, **21**, S983 (1997).

Hauan, S., T. Hertzberg, and K. M. Lien, "Why Methyl *Tert*-Butyl Ether Production by Reactive Distillation May Yield Multiple Solutions," *Ind. Eng. Chem. Res.*, **34**, 987 (1995).

Hoffmaster, W. R., and S. Hauan, "Geometric Insights into Limiting Operating Conditions for Reactive Separation," AIChE Meeting, Reno, NV (2001).

Jacobs, R., and R. Krishna, "Multiple Solutions in Reactive Distillation for Methyl *tert*-Butyl Ether Synthesis," *Ind. Eng. Chem. Res.*, **32**, 1706 (1993)

Lee, J. W., S. Hauan, and A. W. Westerberg, "Graphical Methods for Reactive Distribution in a Reactive Distillation Column," *AIChE J.*, **46**, 1218 (2000).

Lee, J. W., S. Hauan, and A. W. Westerberg, "Feasibility of a Reactive Distillation Column with Ternary Mixtures," *Ind. Eng. Chem. Res.*, **40**, 2714 (2001a).

Lee, J. W., S. Hauan, and A. W. Westerberg, "Graphical Design Applied to MTBE and Methyl Acetate Reactive Distillation Processes," *AIChE J.*, **47**, 1333 (2001b).

Lewis, W. K., and G. L. Matheson, "Design of Rectifying Columns for Natural and Refinery Gasoline," *Ind. Eng. Chem.*, **24**, 494 (1932).

Monroy, R., E. S. Pérez-Cisneros, and J. Alvarez, "A Robust PI Control Configuration for a High-Purity Ethylene Glycol Reactive Distillation Column," *Chem. Eng. Sci.*, **55**, 4925 (2000).

Pérez-Cisneros, E. S., R. Gani, and M. L. Michelsen, "Reactive Separation Systems I. Computation of Physical and Chemical Equilibrium," *Chem. Eng. Sci.*, **52**, 527 (1997).

Pérez-Cisneros, E. S., "Modelling, Design and Analysis of Reactive Separation Process," PhD Thesis, Technical Univ. of Denmark, Lyngby, Denmark (1997).

Pérez-Cisneros, E. S., S. A. Granados-Aguilar, P. Huitzil-Melendez, and T. Viveros-Garcia, "Design of a Reactive Distillation Process for Ultra-Low Sulfur Diesel Production," Computer Aided Chemical Engineering-10, Elsevier, Amsterdam, The Netherlands, p. 517 (2002).

Pilavachi, P. A., M. Schenk, E. S. Pérez-Cisneros, and R. Gani, "Modelling and Simulation of Reactive Distillation Operations," *Ind. Eng. Chem. Res.*, **36**, 3188 (1997).

Rehfinger, A., and U. Hoffmann, "Kinetics of the Methyl Tertiary Butyl Ether Liquid Phase Synthesis Catalysed by Ion Exchange Resin—I. Intrinsic Rate Expression in the Liquid Phase Activities," *Chem. Eng. Sci.*, **45**, 1605 (1990).

Sánchez-Daza, O., and E. S. Pérez-Cisneros, *Chemical and Physical Equilibrium — CPE Program Manual*, Intern. Rep., Univ. Autónoma Metropolitana-Iztapalapa, México City, México (2002).

Seader, J. D., and E. J. Henley, *Separation Process Principles*, Wiley, New York (1998).

Smith, L. A., and M. N. Huddleston, "New MTBE Design Now Commercial," *Hydrocarbon Process.*, **3**, 121 (1982).

Stitt, E. H.,"Reactive Distillation for Toluene Disproportionation: A Technical and Economic Evaluation," *Chem. Eng. Sci.*, **57**, 1537 (2002).

Ung, S., and M. F. Doherty, "Vapour-Liquid Phase Equilibrium in System with Multiple Chemical Reactions," *Chem. Eng. Sci.*, **50**, 23 (1995).

Zhang, T., and R. Datta, "Integral Analysis of Tert-Butyl Ether Synthesis Kinetics," *Ind. Eng. Chem. Res.*, **34**, 730 (1995).

Manuscript received Sept. 4, 2002, and revision received Apr. 1, 2003.